J. Fluid Mech. (1995), *vol.* 293, *pp.* 207–236

Flow regimes and relative permeabilities during steady-state two-phase flow in porous media

By D. G. AVRAAM AND A. C. PAYATAKES

Department of Chemical Engineering, University of Patras *and* Institute of Chemical Engineering and High Temperature Chemical Processes, PO Box 1414, GR 26500 Patras, Greece

(Received 31 May 1994 and in revised form 24 January 1995)

Steady-state two-phase flow in porous media was studied experimentally, using a model pore network of the chamber-and-throat type, etched in glass. The size of the network was sufficient to make end effects negligible. The capillary number, Ca, the flow-rate ratio, r, and the viscosity ratio, κ, were changed systematically in a range that is of practical interest, whereas the wettability (moderate), the coalescence factor (high), and the geometrical and topological parameters of the porous medium were kept constant. Optical observations and macroscopic measurements were used to determine the flow regimes, and to calculate the corresponding relative permeabilities and fractional flow values. Four main flow regimes were observed and videorecorded, namely large-ganglion dynamics (LGD), small-ganglion dynamics (SGD), drop-traffic flow (DTF) and connected pathway flow (CPF). A map of the flow regimes is given in figure 3. The experimental demonstration that LGD, SGD and DTF prevail under flow conditions of practical interest, for which the widely held dogma presumes connected pathway flow, necessitates the drastic modification of that assumption. This is bound to have profound implications for the mathematical analysis and computer simulation of the process. The relative permeabilities are shown to correlate strongly with the flow regimes, figure 11. The relative permeability to oil (non-wetting fluid), k_{ro}, is minimal in the domain of LGD, and increases strongly as the flow mechanism changes from LGD to SGD to DTF to CPF. The relative permeability to water (wetting fluid), k_{rw}, is minimal in the domain of SGD; it increases moderately as the flow mechanism changes from SGD to LGD, whereas it increases strongly as the mechanism changes from SGD to DTF to CPF. Qualitative mechanistic explanations for these experimental results are proposed. The conventional relative permeabilities and the fractional flow of water, f_w, are found to be strong functions not only of the water saturation, S_w, but also of Ca and κ (with the wettability, the coalescence factor, and all the other parameters kept constant). These results imply that a fundamental reconsideration of fractional flow theory is warranted.

1. Introduction

Immiscible two-phase flow in porous media is encountered in several important applications, including primary and secondary oil production, enhanced oil recovery, wetting and drying processes, flow in aquifers, soil reconstitution processes (to remove organic liquid contaminants), etc. An immiscible flow can be a transient displacement (imbibition when a wetting fluid is displacing a non-wetting one, drainage when the non-wetting fluid is displacing the wetting one), or it can be steady state in the narrow sense that both fluids are injected simultaneously at constant flow rates through the porous medium. In the present work we are concerned with the pore-scale mechanisms

and flow regimes of steady-state two-phase flow, and their relation to the relative permeabilities. A major portion of the relevant literature is related to oil production, and for this reason we will use the terms 'water' and 'oil' to denote the wetting and non-wetting fluid, respectively, with the understanding that the results apply to other pairs of immiscible fluids, as well.

Steady-state immiscible two-phase flow is of key importance to the oil industry. The relative permeabilities to oil and water are usually determined under steady-state conditions and then are applied to predict the behaviour of inherently transient displacements, a procedure which is highly questionable. It is necessary to understand the mechanisms responsible for the flow whose macroscopic behaviour is expressed through steady-state relative permeabilities, if proper use of the latter is to be made in practice.

Despite the key importance of steady-state two-phase flow, there are still large gaps in our understanding of it. To begin with, there is considerable confusion in the literature as to which of the system parameters besides the capillary number (viscosity ratio, flow-rate ratio, contact angle, dimensionless geometrical and topological parameters) affect the flow and the relative permeabilities significantly, and in what way. Furthermore, there is a long-standing fundamental misconception concerning the nature of the flow itself. Specifically, there is a long-standing assumption (presumption would be more apt) that the oil flows only through connected pathways, and that disconnected oil is stranded. This assumption was first advanced by Richards (1931) as follows: 'capillary flow takes place through connected configuration, bounded on the one side by the absorbed films in contact with the solid, and on the other by the curved [fluid–fluid] interface', and it has persisted in the literature ever since. For example, Honarpoor & Mahmood (1988) in their relatively recent review article state: 'The effective permeability to a fluid becomes zero while its saturation is finite because the fluids become discontinuous at low saturations'. As we shall see below (see also Avraam *et al.* 1994) this assumption is wrong. Our experiments (and theoretical analysis) show that disconnected oil contributes substantially to the flow of oil. Actually, over a wide range of the system parameters, the flow of oil takes place only through the motion of disconnected bodies of oil (ganglia and/or droplets).

Of course, the motion of oil ganglia has already been studied experimentally (Ng, Davis & Scriven 1978; Rapin 1980; Hinkley, Dias & Payatakes 1987), and theoretically (Ng & Payatakes 1980; Dias & Payatakes 1986*b*; Constantinides & Payatakes 1991), and thus the notion of disconnected oil in motion is nothing new. However, the usual perception is that such phenomena are somehow associated only with tertiary floods that are characterized by high capillary number (Ca) values. The possibility of the existence of low-Ca two-phase flow involving the motion of ganglia was posed in Payatakes & Dias (1984). It is important to realize that the pertinent dimensionless number for mobilization is not Ca, but the ganglion mobilization number Gm. Gm is the ratio of the *actual driving force* exerted on a given oil ganglion by the flowing water to the *actual resistance* offered to the motion of the ganglion by capillary forces. In calculating Gm the size, shape and orientation of the ganglion, as well as the local geometry of the pore network are taken into account (Ng & Payatakes 1980, equation (23); Payatakes & Dias, 1984, equations (17) and (18)). As it turns out, the value of Ca required to mobilize a given ganglion from a given position in a porous medium (by satisfying the local condition $Gm > 1$) is proportional to – among other things – the local relative permeability to water, k_{rw}. There are low-Ca flows of great practical interest in which Gm for many ganglia is larger than unity, and therefore those ganglia move. Such situations arise when k_{rw} is sufficiently small.

In view of the above, it is clear that a systematic parametric study of the flow mechanisms is warranted. The main objectives of the present work are the following:

(*a*) to determine the mechanisms of flow of each phase at the pore level, using suitable model pore networks;

(*b*) to determine the flow regimes of steady-state two-phase flow as a function of the system parameters;

(*c*) to measure the conventional relative permeabilities to both fluids for each set of conditions and to determine the effects of the system parameters;

(*d*) to correlate the macroscopically measured values of the relative permeabilities with the flow mechanisms at the pore scale, and to understand the effects of the system parameters through their effects on the flow mechanisms.

To attain these objectives we conducted 42 experiments, using a model 'chamber-and-throat' pore network. In this set of experiments the capillary number, Ca, the oil-to-water flow-rate ratio, r, and the oil-to-water viscosity ratio, κ, were changed systematically, while all other parameters were kept constant. In each case we observed and videorecorded the flow phenomena at various scales ranging from that of a few pores to that of, say, 10^4 pores, and we measured the conventional relative permeabilities at stationary ('steady state') conditions, k_{ro} and k_{rw}. Each experiment was performed two or three times to ascertain reproducibility. In general, the reproducibility was excellent. We observed a rich flow behaviour, which can be classified roughly in four flow regimes: large-ganglion dynamics (LGD), small-ganglion dynamics (SGD), drop-traffic flow (DTF), and connected pathway flow (CPF). LGD is observed for relatively small to medium Ca values, and small to medium oil saturation, S_o, values. As Ca and/or S_o increase the mean ganglion size decreases and the flow regime becomes SGD. As Ca and/or S_o increase further, the oil becomes disconnected into numerous droplets that have size comparable to the diameter of throats, and the flow regime becomes DTF. Finally, if Ca becomes sufficiently large (in our set of experiments $Ca \gtrsim 5 \times 10^{-6}$) nearly parallel connected pathways of oil spanning the entire model porous medium are formed, in which case the flow is characterized as CPF.

These changes are gradual, and at the borders between flow regimes one observes characteristics of both. Most interestingly, in the case of CPF the fringes of the connected oil pathways are surrounded by drop-traffic flow or small-ganglion dynamics, which can even fill all the spaces among the connected pathways. It should be noted that in the LGD, SGD and DTF regimes all the oil is disconnected, and all oil transport is achieved through the motion of disconnected oil (ganglia or droplets). Even in the case of CPF a significant part of the oil flow rate is due to drop-traffic flow or small-ganglion dynamics in between the pathways.

2. Relative permeabilities

Two-phase flow theory and practice rely heavily on the concept of the relative permeabilities. These quantities, however, are not always clearly defined, nor are they always used consistently. Furthermore, there are cases (such as flow at the front of an advancing flood in displacement processes), where a critical examination of the very concept of relative permeabilities is warranted, before it can be adopted for use.

The parameters that are conventionally employed in the description of two-phase flow in porous media on the macroscopic scale are the relative permeabilities, k_{rw} and k_{ro}, to water and oil, respectively. These parameters appear as proportionality factors in Darcy's law, generalized to the case of multiphase flow (for reviews see Craig 1971; Philip 1970; Wooding & Morel-Seytoux 1976; Adler & Brenner 1988). Whereas

Darcy's law for one-phase flow has received wide validation for numerous types of porous media, further work is needed concerning most aspects of multiphase flow and the proper generalization of Darcy's law.

Relative permeabilities are used as parameters in the *fractional flow theory*, introduced by Leverett (1941) and Buckley & Leverett (1941). This theory has been widely used and tested in immiscible displacement and simultaneous two-phase flow processes (Osoba *et al.* 1951; Terwilliger *et al.* 1951; Jones-Parra & Calhoun 1953; Rapoport & Leas 1953; Levine 1954; Heavyside, Black & Berry 1983), but it has also received much criticism. The criticism has been addressed mainly towards the applicability of the concept of relative permeabilities in immiscible displacement processes (Jones & Roszelle 1978; Heavyside *et al.* 1983), the assumptions involved in their experimental measurement (Rose 1991), and on the adequacy of the conventional relative permeabilities to describe two-phase flow processes in porous media (Rose 1988). There are also doubts about the practical usefulness of the conventional relative permeabilities, when they depend (as they strongly do) on the fluid flow rates and on the specific manner in which the fluids are distributed in the pore space.

In addition to the above considerations, several experimental and theoretical studies (Raats & Klute 1968; Rose 1972, 1988, 1990; de Gennes 1983; de la Cruz & Spanos 1983; Auriault 1987; Auriault, Lebaigue & Bonnet 1989; Kalaydjian 1987, 1990) have shown that the interactions between the two fluids can be important, and that additional interaction coefficients (cross-terms) must be included in the generalized Darcy's law for two-phase flow. At present there is no well-established method that can determine the cross-terms directly from data taken during two-phase flow in porous media. For this reason, the experimental data are still being analysed in terms of the conventional relative permeabilities.

There are many uncertainties concerning the parameters that affect the conventional relative permeabilities. The effects of the following parameters have been studied in the literature: saturation of fluids (Johnson, Bossler & Naumann 1959; Naar, Wygal & Henderson 1962), capillary number, Ca, flow-rate ratio, r (Leverett 1941; Sandberg, Gournay & Sippel 1958; Taber 1958; Lefebvre du Prey 1973; Amaetule & Handy 1982; Fulcher, Ertekin & Stahl 1985), viscosity ratio, κ (Yuster 1951; Odeh 1959; Lefebvre du Prey 1973; Fulcher *et al.* 1985), wettability or equilibrium contact angle, θ_e (Geffen *et al.* 1951; Owens & Archer 1971; McCaffery & Bennion 1974), distribution of fluids, history of saturation change, pore geometry and topology (Jerault & Salter 1991).

Two main methods are used for the experimental determination of the conventional relative permeabilities. The first is the steady-state method, which is based on simultaneous injection of both fluids, and the second is the unsteady-state method, which is based on immiscible displacement experiments. Each method adopts several assumptions, some of which are neither clearly stated nor well understood (Rose 1991).

The unsteady-state method is often considered to be more suitable for the determination of relative permeabilities, when these are to be used to predict the evolution of waterflood processes, because of a degree of similarity between the experimental and field flows. The data are the effluent volumes of water (water cut in the effluent stream) and the pressure gradients in the water as a function of time. The data are analysed based on fractional flow theory and its extensions (Welge 1952; Johnson *et al.* 1959; Jones & Roszelle 1978). These methods are based on the postulate that capillary pressure is negligible compared to the viscous forces, an assumption that may not be valid under typical waterflood conditions (Bentsen 1978). In addition,

operational difficulties, capillary end effects, viscous fingering and a short time span between front breakthrough and flood completion make the results uncertain, although these have substantial qualitative value (Honarpoor & Mahmood 1988). The main advantage of the method is the significant reduction of the experimental time needed to determine the relative permeabilities over the complete range of fluid saturation values. Continual research keeps making improvements in the efficacy of this method.

The steady-state method is thought to produce more reliable experimental data than those of the unsteady state, because it is based on the direct application of the generalized Darcy's law. The two immiscible fluids are injected simultaneously at constant flow rates (or pressures) into the porous medium until the flow reaches equilibrium. Equilibrium here must be considered as the dynamic result of the interplay of several viscous and capillary flow phenomena. At these 'equilibrium' or 'steady-state' flow conditions the macroscopically stable (but microscopically fluctuating) flow rates, pressure drops and fluid saturations are measured and correlated using Darcy's law. This flow is better characterized as *stationary*, in a stochastic sense, rather than as 'steady state'. The most important operational problems encountered with this method include capillary end effects, hysteresis, scaling effects and the long times that are needed before a stationary flow is attained. Several variations of the method have been proposed aiming to establish capillary equilibrium between the fluids, and to reduce end effects. Among these variations, Hassler's, the dispersion-feed and the Penn-State methods are the most important. A suitable combination of these methods is used in the present work.

The most serious source of error is the capillary end effects, which cause a capillary pressure gradient along the porous medium. In such a case the conventional generalization of Darcy's law is no longer valid. The phenomenon occurs because water prefers to remain in the narrow capillary pores near the exit of the porous medium rather than to enter into the non-capillary space downstream of the exit. Another error is made by attributing the pressure drop of one phase (usually that of oil) to both phases, thus ignoring the difference caused by the capillary pressure. Standard techniques are used to minimize end effects. To begin with, long cores of the porous medium are used. Secondly, porous plates are placed in contact with the inlet and outlet faces of the core, as flow distributors. These plates can be made from porous material other than that of the porous medium, but their wettability has to be similar to that of the rock (a condition that is usually hard to satisfy). Thirdly, one or both fluids are fed through the inlet porous plate in order to be mixed properly before entering into the core. In Hassler's technique only the wetting phase passes through the inlet porous plate, whereas the non-wetting phase is fed directly to the inlet core face. The pressure drop of each phase can be measured separately, thus, taking into account the effects of capillary pressure. In the Penn-State method both fluids are fed through the inlet porous plate. It is feasible to measure pressure drops separately in both phases using pressure taps with suitable hydrophilic and oleophilic semipermeable membranes at the points of contact with the porous medium (Levine 1954).

Other methods (Hafford, dispersed feed, stationary liquid, etc) try to reduce or eliminate the capillary end effects in a way that may alter the original flow pattern and distribution of the fluids. For example, they use high flow rates, or they keep one phase (usually the oil) stationary and they measure the relative permeability of the other phase at various saturation levels. If the distribution of the fluids in the pore space and the configuration of the fluids at pore level are to be taken into account, then these methods have to be avoided.

It is worth noting that certain assumptions are implicitly made in the Richards–Hassler method (on which all variations of the steady-state method are based). Some of these have been taken for granted, traditionally, though a clear statement to this effect is not easy to find. Rose (1991) presented a valuable critical review of the several questionable assumptions involved in determining relative permeabilities. Interestingly, the erroneous assumption concerning the lack of mobility of disconnected oil, that was discussed above, was not included explicitly even in Rose's otherwise comprehensive list. As we will see below, disconnected oil can contribute substantially, or even totally, to the transport of oil. Hence, the detailed distribution of fluids in the pore space, as well as the specific mechanisms of fluid flow at the pore scale and the macroscopic scale, under dynamic 'steady-state' flow conditions, must be taken into account carefully, if a clear connection between them and any macroscopically measured quantity, such as relative permeabilities, is to be made. To date, little information about these fundamental aspects of two-phase flow have appeared in the literature, though it is of crucial importance to gain insight into these processes (Payatakes & Dias 1984).

3. Materials and methods

3.1. *Model porous medium*

All the experiments of this work were made using one and the same model porous medium, so that the observed variations can be attributed to changes in the physical and operational parameters only. The model porous medium is a network of the chamber-and-throat type etched in glass, and its characteristics are such that it gives a relatively simple (but not overly simplified) representation of a reservoir sandstone (see figures 4, 5, 6 and 7). The network has a two-dimensional skeleton, but – as has been shown in Avraam *et al.* (1994) – the qualitative aspects of the flow apply to three-dimensional topologies as well. In pore networks with three-dimensional topology the flow regimes reported here are expected to be somewhat displaced in the parameter space $\{S_w, Ca, \kappa, \ldots\}$, but the essence of the matter remains the same.

The model was constructed with a photoetching technique similar to that described in Vizika & Payatakes (1989). The skeleton of the network is a square lattice with node-to-node distance of 1221 μm, and arranged so that the macroscopic flow direction is parallel to one family of diagonals. The network comprises 11300 chambers and 22600 throats. The chamber size (diameter) distribution and the throat size (width) distribution have discrete (composed of five classes each) nearly normal size distributions with mean values $\langle D_c \rangle = 560$ μm, $\langle D_t \rangle = 112$ μm, and standard deviations equal to 1/4 of the corresponding mean values. Mirror images of the network are etched on two glass plates, which are then aligned precisely and sintered in a programmable muffle furnace. The maximum pore depth is nearly uniform with mean value 140 μm. Owing to the characteristics of the wet etching process, the cross-sections of the throats are eye-shaped, as in Vizika & Payatakes (1989) (see also, Chatzis, Morrow & Lim 1983). The top-view porosity of the networks is 0.25. The values of the geometrical parameters of the pore network model are summarized in table 1.

Each end of the main pore network is extended with three triangular segments, which serve as flow distributors, figures 1 and 2. Two holes of diameter 5 mm are drilled (through the top glass plate) near the two sides of each triangular entrance flow distributor, figure 1. These holes serve as ports for the injection of the two fluids. A single similar hole is drilled at the end of each exit flow distributor to serve as outlet

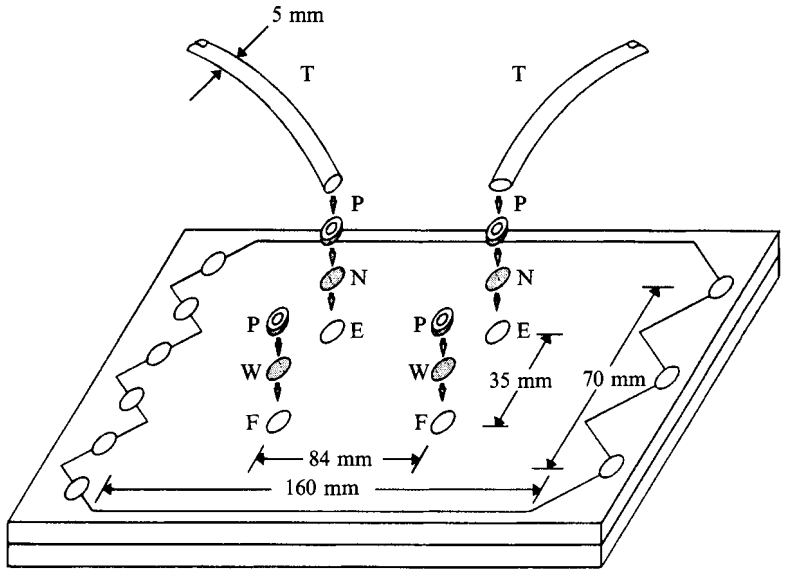

FIGURE 1. Drawing of the large planar model porous medium used in the experiments. E, F: oil and water pressure taps; W, N: circular disks of the water and the oil semi-permeable membranes; P: plastic O-rings; T: plastic tubes connecting the pressure taps with the pressure transducers.

Chamber diameter (μm)	280	420	560	700	840
Throat width (μm)	56	84	112	140	168
Frequency of appearance (%)	16.0	21.0	26.0	21.0	16.0

TABLE 1. Geometrical parameters of the pore network model: mean chamber to mean throat size ratio, $\zeta = 5:1$; length of periodicity, $l = 1221$ m; planar porosity, $\epsilon = 0.25$; coordination number, $\sigma = 4$; angle between pore network axis and flow direction, $\phi = 45°$; mean pore depth, $w = 140$ μm; cross-sectional area of the model porous medium, $A = 128.2$ mm^2; absolute permeability, $k = 9.02$ Da ($= 8.90$ μm^2).

for both fluids. This arrangement was found to give very good flow distribution over the entire pore network. Another four holes of diameter 5 mm were drilled through the top glass plate, as pressure taps, at the corners of a centrally located rectangular region with length 84 mm in the main flow direction and width 35 mm, figure 1. This central rectangle is the region in which all measurements were made. The two pairs of pressure taps are used to measure the pressure drops in each of the two fluids. To achieve this, the ends of the tubes that are intended for the measurement of the water pressure are sealed with a water-permeable/oil-impermeable membrane, whereas the ends of the tubes that are intended for the measurement of the oil pressure are sealed with an oil-permeable/water-impermeable membrane, figure 1.

3.2. *Experimental apparatus*

Flow observations and relative permeability measurements were made during 'steady-state' two-phase flow. The two fluids are injected simultaneously with constant flow rates in the porous medium until dynamic equilibrium (i.e. a stationary process) is attained. Fluid saturations, flow rates and pressure drops are measured (as described below) and Darcy's law, written for each of the two fluids, is used to obtain the relative permeabilities (see below).

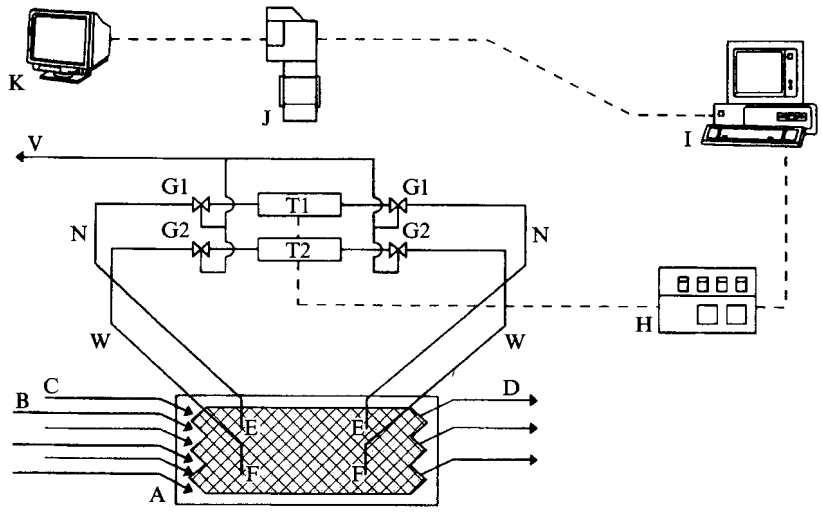

FIGURE 2. Drawing of the experimental apparatus. Dashed lines represent electrical connections and solid lines represent hydraulic connections. A: planar model porous medium; B, C: inlet ports for the oil and the water, respectively; D: outlet ports for the fluids; E, F: pressures taps; N, W: tubes connecting the pressure taps with the pressure transducers; T1, T2: pressure transducers; G1, G2: three-way valves; V: venting line; H: digital pressure indicator; I: personal computer; J: videocamera; K: monitor.

Figure 2 gives a schematic depiction of the experimental apparatus, whereas figure 1 shows details of the tubing connections. The pore network model A is connected with two pumps of the syringe infusion-withdrawal type (Harvard Apparatus, Models 915A and 940A), which inject the fluids into the pore network model at preselected flow rates through three tube connections B for the wetting fluid, and another three connections C for the non-wetting fluid. Measurements and observations are made in the region EE–FF, which is sufficiently removed from the boundaries to give two-phase flow virtually free from end effects. The triangular regions near the fluid inlets and the rectangular one up to the region EE–FF act as flow distributors, to minimize inlet effects. Similar regions are employed on the outlet side to minimize outlet effects. The fluids flow out of the pore network model through three tube connections D, and are collected in a flask. This design utilizes ideas from the Penn-State and dispersed-feed methods (Morse, Terwilliger & Yuster 1947; Osoba *et al.* 1951; Richardson *et al.* 1952).

The pressure drops in the two fluids are measured separately. Two tube connections E–N–G1–T1 connect the pore network model with the differential pressure transducer T1 (Druck, Model PDCR 120/7WL) through the tubes N, which are filled with the non-wetting fluid. The same is done for the wetting fluid, and two tube connections F–W–G2–T2 connect the pore network model with the differential pressure transducer T2. The tubes W are filled with the wetting fluid. G1 and G2 are three-way valves allowing the transducers T1 and T2 to be connected either with the pore network model, or with the vent line, V, through the connections T1–G1–V and T2–G2–V.

In order to measure the pressure drops in both phases separately, special pressure taps were used at the points E and F, where the pore network model is connected to the tube lines N and W, respectively. The pressures in the non-wetting phase were measured at the points E through two pressure taps, sealed with oleophilic membranes (Gore, membranes Goretex 0.1 μm, and Millipore, membranes GVHP 04700 0.22 μm).

The pressure taps for the wetting phase, placed at the points F, are sealed with hydrophilic membranes (Millipore, membranes GVWP 04700 0.22 μm). Four circular disks of diameter 5 mm were cut from the appropriate membrane sheets and were placed at the bottom of the pressure tap wells. The membrane disks were then pressed in place with plastic O-rings driven in with a rod, and the tubes N and W were inserted tightly over them, as shown in figure 1. In this manner, each phase inside the tube lines W and N becomes isolated from the other phase, while it remains in hydraulic contact with the same phase flowing inside the pore network model, through the membrane. Thus, the true pressure drops of the non-wetting fluid (EE) and the wetting fluid (FF) were measured. This technique has been used in Richardson *et al.* (1952) and in Levine (1954). In order to obtain pressure measurements that are representative of the flow conditions in the porous medium, the pressure taps E and F were designed sufficiently large, so that each of them is in direct contact with 15 chambers. The distance, d, between the points at which pressure measurements are taken is much larger than the characteristic pore dimension (see Whitaker 1986). Here $l_b \approx 0.11$ mm $\ll d = 84$ mm.

A central idea behind the present work is to relate the flow phenomena observed at the pore scale with macroscopic quantities such as the relative permeabilities. A CCD Videocamera, J (Panasonic WVP-F10 CCD Videocamera PAL), with a special magnifying lens (Nikon ED, AF Nikkor 80–200 mm, 1:2.8) was used to observe and record the flow phenomena at the pore and mesoscopic scale, during 'steady-state' two-phase flow, while macroscopic flow rate and pressure drop measurements were being taken continuously. Image data and pressure difference data were transmitted continuously to the host computer, I (PC 386DX, 40 MHz). Images were taken continuously (real-time image grabbing) from the flow area EE–FF at appropriate magnification levels, and they were sent to an image analysis card (Imaging Technology, Itex VP-1320-768-E-AT, 50 Hz line frequency, 15 MHz sample frequency, 768×512 pixel standard image size), which is installed in the host computer. The images were digitized and the mean saturation value and the ganglia size distribution were obtained as functions of position and time. In addition to these measurements, key flow phenomena occurring at the pore scale (e.g. the motion, the breaking, the stranding and the coalescence of ganglia) were observed in detail, while the corresponding macroscopic flow patterns were identified. The flow images were monitored with the help of the monitor, K (Sony, Trinitron Color Video Monitor PVM-2010QM), recorded and stored on videotapes, for further studies (Sony, U-matic Videocassette Recorder VO-5800 PS). The pressure difference data were transmitted continuously to the computer through the pressure indicator, H (Druck, Model DPI 420, Multichannel Pressure Indicator). The mean values of pressure differences were combined with the fluid flow rates to obtain the relative permeabilities to both phases, which were correlated with the mean saturation value and the pore-scale flow mechanisms.

3.3. *Experimental procedure*

Initially, the glass pore model is saturated with oil. The air is removed from the model and from all inlet and outlet tubes, B, C and D, using continuous flow of the oil at a high flow rate. At this stage the oil is injected through all inlet connections B and C, driven by the two syringe pumps, and flows through the model pore network A to the exit tubes, D.

Next, the transducers T1 and T2 are prepared to be connected with the model pore network A. With the help of the three-way valves G1 and G2, the tubes E–N–G1–T1 and F–W–G2–T2 are filled with oil and water, respectively. Air is carefully removed from all these tubes with the help of the additional connections T1–G1–V and

T2–G2–V. A vacuum pump is used to evacuate these connections, so that G1–T1 and G2–T2 become entirely free from air bubbles while they are being filled with the fluids. Then, tubes N and W become connected with the glass model at the pressure taps E and F.

Flow-rate values are selected to obtain the desired ratio, and the two fluids begin to be fed into the pore network model. In most cases, the initial phase of the experiment consists in the formation of a front of oil being displaced, while new oil also enters into the pore model behind the front. After a while, the two phases become spread out over the entire pore network, and in all subsequent stages they flow simultaneously through every cross-sectional area. This procedure corresponds to *initial imbibition* conditions. This is important to remember, because there is considerable difference in the relative permeabilities measured in imbibition and drainage processes due to hysteresis effects (Craig 1971; Jerault & Salter 1990). The length of time required to establish 'steady-state' ranges from several hours to a few days, depending on the flow rates and physicochemical properties of the fluids. When the mean pressure differences of both phases become stabilized, 'steady-state' measurements are taken. The pressure drop in each phase is obtained as the time average of the corresponding continuous signal. Here, it must be noted that even at 'steady state' the pressure drop signals show a very noisy (chaotic?) behaviour around the corresponding mean values. This is not an artifact; rather, it is caused by the virtually chaotic passage of ganglia/droplets of oil through most regions of the pore network. Fortunately, despite the noisy behaviour of the two signals, reliable and consistent time-averaged values are obtained. The saturation is obtained by measuring the void-area fraction occupied by oil, through appropriate processing of the digitized image data.

Each experiment was performed two or three times, and excellent reproducibility was found in all cases. Furthermore, the flow phenomena at pore scale and also the macroscopic flow patterns were found to be the same under similar flow conditions.

Before and after each experiment, the glass pore model is cleaned thoroughly, as follows. The model is flooded with deionized water followed by sulphuric acid, which is left in the pores for two or three hours. After that, the model is flooded thoroughly with deionized water, followed with acetone, and it is dried with a current of dry air. This procedure restores the initial wettability of the glass model, which can change during long experiments. It is to be noted that changes in the wettability, during any experiment, effect changes in the pressure differences, and also in the pore-scale phenomena, so that they can be detected readily. Whenever a change in wettability was detected in one of our experiments, that particular run was rejected and the experiment was repeated from the beginning, starting with thorough cleaning of the glass model. Another necessary precaution that was taken was to change all tubing connections with new ones before every experiment.

3.4. *Design of experiments*

Dimensional analysis shows that the steady-state relative permeabilities (in a given porous medium) are functions of several parameters,

$$k_{ro} = k_{ro}(S_w, Ca, r, \kappa, \cos\theta_a, \cos\theta_r, Co, Bo;\ \boldsymbol{x};\ \text{flow history}), \tag{1}$$

$$k_{rw} = k_{rw}(S_w, Ca, r, \kappa, \cos\theta_a, \cos\theta_r, Co, Bo;\ \boldsymbol{x};\ \text{flow history}), \tag{2}$$

where S_w is the water saturation, Ca is the capillary number (which is defined as $Ca = \mu_w q_w/\gamma_{ow} wl$, where μ_w is the viscosity of 'water', q_w is the volumetric flow rate of 'water', γ_{ow} is the interfacial tension, w is the width of the network, and l is the node-

r	q_o (ml min^{-1})	q_w (ml min^{-1})	S_w(%)	ΔP_o (mbar)	ΔP_w (mbar)	k_{ro}(%)	k_{rw}(%)
			(*a*) $Ca = 1.19 \times 10^{-7}$				
$\kappa = 3.35$							
0.10	0.0024	0.0243	61.03	20.38	14.20	0.4548	1.9722
0.45	0.0110	0.0243	52.79	23.89	17.39	1.7782	1.6104
1.14	0.0276	0.0243	48.41	25.70	20.85	4.1476	1.3432
2.27	0.0552	0.0243	44.04	29.12	24.81	7.3209	1.1336
11.35	0.2760	0.0243	33.74	44.79	36.89	23.7982	0.7592
$\kappa = 1.45$							
0.10	0.0024	0.0243	61.73	16.73	15.22	0.2392	1.8400
0.45	0.0110	0.0243	56.21	21.66	16.50	0.8468	1.6973
1.14	0.0276	0.0243	51.64	22.27	22.24	2.0665	1.2592
2.27	0.0552	0.0243	46.17	27.34	24.87	3.3665	1.1261
11.35	0.2760	0.0243	35.42	42.32	38.10	10.8745	0.7350
$\kappa = 0.66$							
0.25	0.0024	0.0097	63.08	22.08	21.56	0.1812	1.1418
0.43	0.0042	0.0097	61.28	26.20	25.27	0.2673	0.9742
1.08	0.0105	0.0097	57.47	23.95	26.53	0.7310	0.9279
2.84	0.0276	0.0097	50.51	26.79	29.87	1.7178	0.8242
10.80	0.1050	0.0097	43.03	37.61	43.59	4.6551	0.5648
			(*b*) $Ca = 1.19 \times 10^{-6}$				
$\kappa = 3.35$							
0.11	0.0276	0.2430	62.94	41.82	38.81	2.5488	7.2160
0.45	0.1110	0.2430	57.09	50.57	45.27	8.4767	6.1863
1.14	0.2760	0.2430	50.47	53.97	51.97	19.7502	5.3887
2.27	0.5520	0.2430	45.77	72.46	61.11	29.4209	4.5828
4.54	1.1040	0.2430	38.85	125.61	110.25	33.9438	2.5402
$\kappa = 1.45$							
0.11	0.0276	0.2430	63.54	40.85	39.63	1.1266	7.0667
0.45	0.1110	0.2430	58.54	49.28	46.57	3.7557	6.0136
1.14	0.2760	0.2430	53.79	53.61	52.54	8.5844	5.3303
2.27	0.5520	0.2430	48.82	70.93	61.12	12.9764	4.5083
4.54	1.1040	0.2430	41.15	83.63	124.80	22.0116	2.2440
$\kappa = 0.66$							
0.25	0.0240	0.0972	64.23	32.41	39.44	1.2347	6.2547
0.57	0.0552	0.0972	61.56	52.83	44.35	1.7422	5.5662
1.08	0.1050	0.0972	58.83	51.42	51.64	3.4049	4.7770
2.84	0.2760	0.0972	53.24	63.98	61.85	7.1930	3.9881
11.36	1.1040	0.0972	44.03	107.14	117.40	17.1815	2.1012
			(*c*) $Ca = 4.75 \times 10^{-6}$ (5.94×10^{-6} for $\kappa = 0.66$)				
$\kappa = 3.35$							
0.11	0.1110	0.9720	65.61	77.85	85.77	5.5066	13.0606
0.57	0.5520	0.9720	59.52	93.42	106.84	22.8200	10.4849
1.14	1.1040	0.9720	54.96	116.88	120.99	36.4792	9.2587
2.84	2.7200	0.9720	46.83	160.18	166.63	65.5808	6.7227
$\kappa = 1.45$							
0.11	0.1110	0.9720	67.03	84.26	90.14	2.1966	12.4274
0.57	0.5520	0.9720	62.25	95.77	110.42	9.6107	10.1450
1.14	1.1040	0.9720	57.64	116.85	121.73	15.7538	9.2024
2.84	2.7200	0.9720	50.56	193.56	168.64	23.4314	6.6426
$\kappa = 0.66$							
0.23	0.1110	0.4860	68.04	115.92	108.79	1.5966	11.3376
0.57	0.2760	0.4860	65.19	127.98	137.24	3.5959	8.9873
1.14	0.5520	0.4860	61.57	139.17	159.53	6.6136	7.7316
2.27	1.1040	0.4860	57.62	179.64	184.22	10.2473	6.6954

TABLE 2. Values of the flow parameters (Ca, κ, r, q_o, q_w) and of the measured variables (S_w, ΔP_o, ΔP_w, k_{ro}, k_{rw})

Non-wetting fluid Wetting fluid	Fluid system 1: n-Hexadecane Deionized water	Fluid system 2: n-Dodecane Deionized water	Fluid system 3: n-Dodecane Deionized water + 30% glycerol
μ_o (Pas)	0.00315	0.00136	0.00136
μ_w (Pas)	0.00094	0.00094	0.00207
$\kappa = \mu_o/\mu_w$	3.35	1.45	0.66
ρ_o (kg m^{-3})	774	730	730
ρ_w (kg m^{-3})	995	995	1066
σ_{ow} (mN m^{-1})	25	25	22
θ_e (degrees)	42	40	40

TABLE 3. Physicochemical properties of fluid systems

to-node distance of the pore network), $r(= q_o/q_w)$ is the flow-rate ratio, $\kappa(= \mu_o/\mu_w)$ is the viscosity ratio, θ_a and θ_r are the advancing and receding contact angles (here assumed equal to their equilibrium values, for simplicity), and *Bo* is the Bond number. *Co* is the *coalescence factor*, and it is defined as the effective probability of coalescence given a collision between two ganglia, or other bodies of oil. (This parameter is of fundamental importance, and yet it is nearly always overlooked. The behaviour of inherently unstable fluid–fluid systems flowing in porous media is substantially different from that of stabilized systems.) The parameter vector $\boldsymbol{x}$ stands for all those dimensionless topological and geometrical parameters that affect the flow (porosity, genus, coordination number distribution, normalized chamber size distribution, normalized throat size distribution, throat size correlation coefficients, etc.) Finally, 'flow history' denotes the manner in which the steady-state conditions have been reached, for example, whether through initial imbibition or drainage. Flow history affects the distribution of the two fluids within the pore structure at the pore level and, consequently, the relative permeabilities.

Clearly, a complete parametric study in which all the parameters are to be changed in a systematic way is a task that will require very much effort. In the present work we make a first attempt to determine the flow regimes (namely, parameter regions in which various flow mechanisms prevail) and to measure the corresponding relative permeabilities by changing systematically S_w, *Ca*, r, and κ, while keeping $\boldsymbol{x}$ constant (we used the same model porous medium throughout), θ_a and θ_r virtually constant, and the 'flow history' constant (we followed the same experimental protocol in all experiments). In all our experiments (42, each performed at least twice) the model porous medium was horizontal and *Bo* played no role. The coalescence factor *Co* is extremely hard to measure and control precisely. In all our experiments *Co* was large (coalescence was prompt), because no surfactants were used and the interfacial tension was large, $\sigma_{ow} = 22$–25 mN m^{-1} (Constantinides & Payatakes 1991).

In addition to (1) and (2), a similar equation can be written relating the 'steady-state' mean water saturation S_w with the system parameters

$$S_w = S_w(Ca, r, \kappa, \cos\theta_a, \cos\theta_r, Co, Bo; \boldsymbol{x}; \text{flow history}). \tag{3}$$

Consequently, the relative permeabilities of the fluids, k_{ro} and k_{rw}, can be presented conveniently as functions of S_w, *Ca*, and κ, while keeping all other parameters constant, along with the presentation of the water saturation, S_w, as a function of *Ca*, r and κ.

The values of Ca, r, κ, and S_w in our experiments are summarized in table 2. The values of the rest of the parameters, which were kept constant (or nearly so) are given in table 3.

4. Experimental results

4.1. *Steady-state two-phase flow regimes*

In most of the experiments of the present work the oil was completely disconnected, while the water was connected. Thus, whereas the water flowed through continuous pathways, the flow of oil took place entirely through the motion of oil ganglia and/or droplets. Only for relatively high Ca values (say, higher than $\sim 5 \times 10^{-6}$ to 10^{-5}) were continuous oil pathways observed. In the latter case the oil in the regions among the continuous oil pathways was again disconnected in droplets and ganglia, the motion of which seems to contribute substantially to the oil flow rate.

Four main flow regimes can be defined, based on the mean size of the *mobilized* ganglia, the preponderance of droplets, and the presence or absence of connected oil pathways. These regimes are: large-ganglion dynamics (LGD), small-ganglion dynamics (SGD), drop-traffic flow (DTF), and connected pathway flow (CPF).

Before proceeding with a detailed description of the flow phenomena in each regime, it is useful to construct a map of flow regimes, figure 3. This map is somewhat rough, since the boundaries on each of the three planes (for $\kappa = 0.66$, 1.45, and 3.35) have been drawn based on 14 flows (corresponding to 14 different pairs of Ca and S_w values) each. This choice, however, has been imposed by the fact that these experiments are very time consuming, and that each of the 42 experiments was repeated at least once, usually twice, to ascertain its reproducibility. It is important to note that the boundaries are fuzzy, and that the transition from any flow regime to a neighbouring one is gradual. The boundaries in figure 3 are drawn so as to pass halfway between the (Ca, S_w) points that correspond to the experimental observations. A description of the main characteristics of each flow regime is given below.

In *large-ganglion dynamics* (LGD) the oil is totally disconnected in the form of ganglia with mean size of the moving ganglia larger than *ca.* 10 chambers. Ganglion dynamics is the term introduced by Payatakes, Ng & Flumerfelt (1980) and Payatakes (1982) to describe two-phase flow in which the non-wetting phase flows in the form of discrete ganglia. In the general case the population of the ganglia is composed of two interacting subpopulations, that of the moving ganglia and that of the stranded ganglia. The interaction between the two subpopulations is complex. Moving ganglia may become stranded by arriving at a difficult passage, or they fission into daughter ganglia which, being shorter, become stranded more easily. On the other hand, moving ganglia can collide with others, which are either stranded or moving, and coalesce with them to form larger ganglia, which usually keep moving, at least for a small distance. Stranded ganglia can become mobilized through collision/coalescence with moving ones, or by a favourable change of the local flooding conditions (namely, by an increase of the local value of the ganglion mobilization number Gm; see Payatakes & Dias 1984; also Ng & Payatakes 1980).

For all the fluid systems investigated ($\kappa = 0.66$, 1.45, 3.35), LGD appeared when a combination of low Ca values ($Ca = 10^{-7}$ and 10^{-6}) with low r and, hence, high S_w values ($S_w > 50\,\%$) was used. This happens because low injection rates of the two fluids favour the motion of the larger ganglia while the smaller ones rarely move and are usually stranded. Furthermore, these flow conditions are less favourable to the fission of ganglia. It is interesting to note that as the viscosity ratio κ decreases, LGD prevails

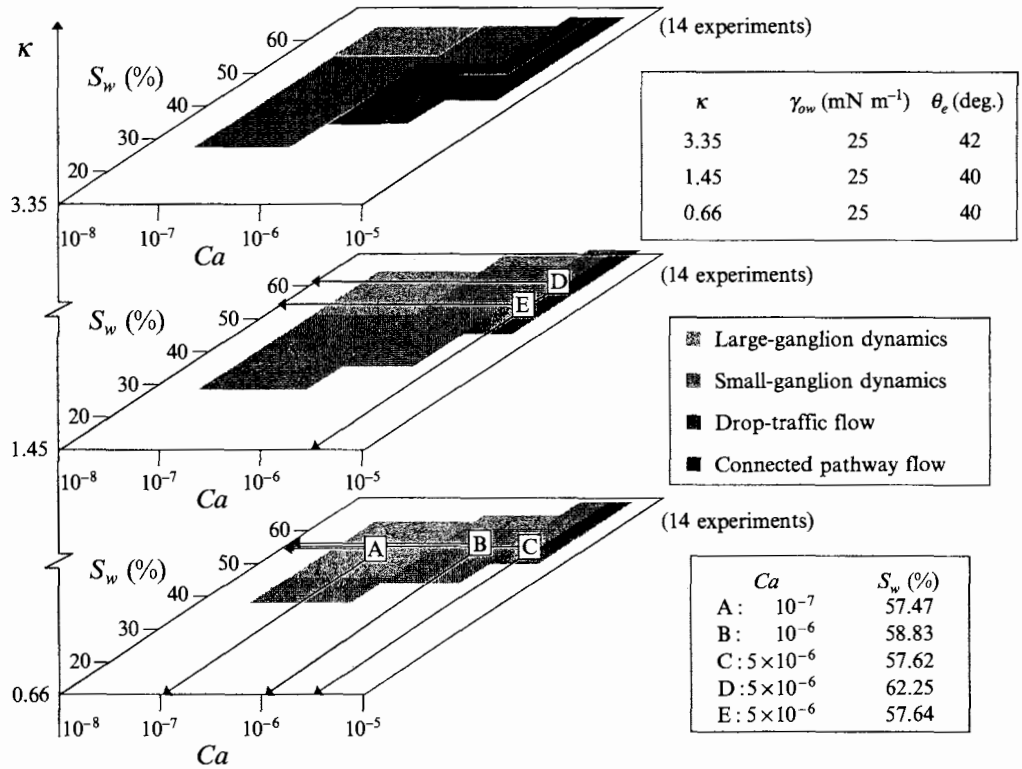

FIGURE 3. Map of the experimentally observed flow regimes in terms of Ca, S_w and κ. The three planes correspond to the viscosity ratio values $\kappa = 3.35$, 1.45, 0.66. For each κ value the flow regimes are shown as domains in the Ca and S_w plane. The boundaries between flow regimes are to be considered as fuzzy.

in broader areas of the system parameters, specifically at even higher values of Ca and lower values of S_w. This happens because, as the viscosity ratio decreases, large oil ganglia fission with greater difficulty. Conversely, at constant Ca, smaller ganglia are produced as r increases, that is, when S_w decreases.

Figure 4 shows successive snapshots from the experiment that corresponds to the point A in the diagram of figure 3. These pictures are typical of LGD. Figure 4(*d*) shows that at the scale of hundred of pores the fluid distribution is homogeneous, as expected from a macroscopically homogeneous pore network. Oil ganglia of different sizes, including small ones, are present and the smaller sizes prevail. However, the small ganglia are mostly stranded, while the larger ones pass slowly among them interacting with those small and large ganglia that they meet on their way. The moving ganglia seem to follow some preferred paths, which, however, are not permanent, but they become active or inactive in a fluctuating manner.

The situation is akin to the fluctuations observed in some steady-state two-phase flow experiments (Craig 1971), but here it is observed in the case of ganglion dynamics, rather than in the case of flow through connected pathways.

Small-ganglion dynamics (SGD) is similar to LGD in every respect, with the sole exception that the mean size of the moving ganglia is substantially smaller than 10 chambers. Of course, the transition from LGD to SGD is gradual, and the boundary between the two is fuzzy. SGD arises when both fluid flow-rates, q_o and q_w, become

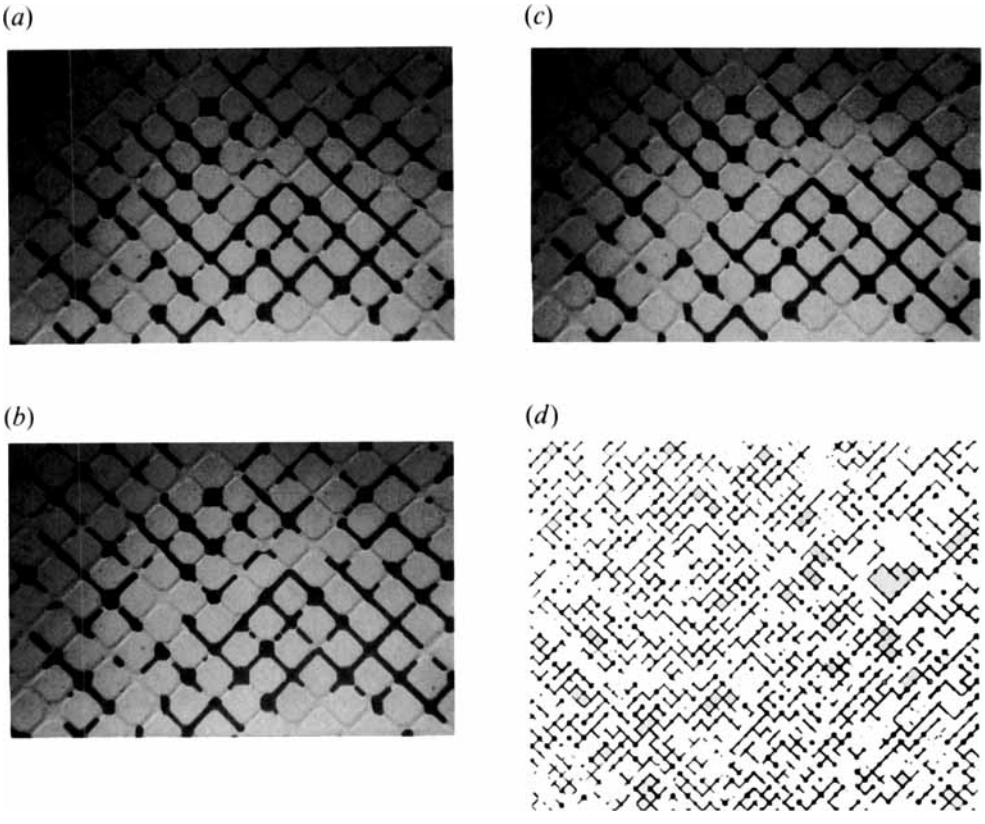

FIGURE 4. Large-ganglion dynamics: (*a–c*) three successive snapshots from the experiment corresponding to the point A in figure 3: (*d*) a snapshot from the same experiment taken with lower magnification to show the homogeneous distribution of the fluids at the macroscopic scale. (The segment of the pore network shown here is approximately one half of the central region over which quantitative measurements were made.)

larger than those that lead to LGD. Figure 3 shows the domain of SGD for three different values of the viscosity ratio κ. In each case the domain of SGD is adjacent to that of LGD, and corresponds to larger values of Ca and/or smaller values of S_w. As the viscosity ratio decreases, the domain of SGD shifts to larger values of Ca and smaller values of S_w. The domain of SGD increases as the viscosity ratio κ decreases from 3.35 to 1.45, whereas it decreases again, slightly, as κ decreases from 1.45 to 0.66.

Successive snapshots from the experiment that corresponds to the point B in figure 3 are shown in figure 5. The flow regime here is SGD. Again, the macroscopic distribution of water and oil is uniform over the entire pore space (figure 5*d*) in the area of measurements (figure 1). Many small ganglia are in motion throughout the pore network. Some large ganglia are created from time to time, but these fission quickly into smaller ones because of their relatively high velocity (Hinkley, Dias & Payatakes 1982). Under these conditions, breakup of the large ganglia and collision and coalescence of the small ganglia produce a population of small and medium-sized ganglia. If one causes a further increase of Ca and/or a decrease of S_w, the process of breakup predominates over that of collision and coalescence and the flow pattern shifts into the drop-traffic flow regime.

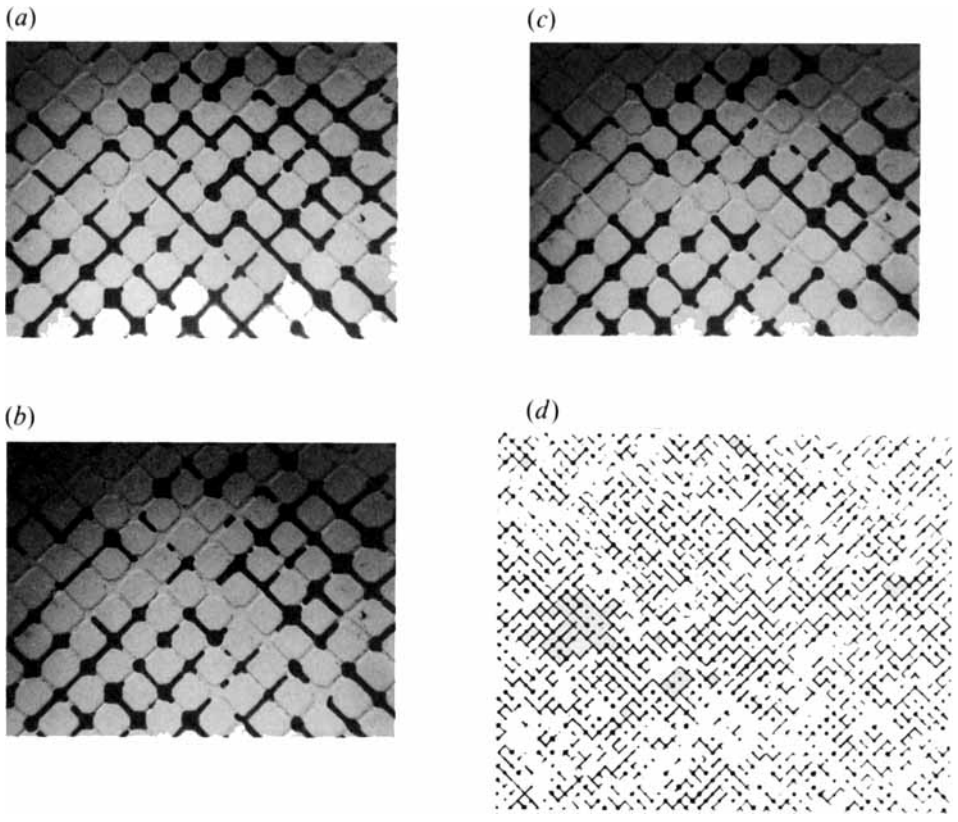

FIGURE 5. Small-ganglion dynamics: (*a–c*) three successive snapshots from the experiment corresponding to the point B in figure 3; (*d*) a snapshot from the same experiment taken with lower magnification to show the homogeneous distributions of the fluids at the macroscopic scale.

The term *drop-traffic flow* (DTF) is introduced here to describe the steady-state two-phase flow regime, in which most of the oil is disconnected in the form of droplets that have sizes comparable to the diameters of the throats of the pore network. (Of course, a few small ganglia, usually stranded in 'tight' places, are still observed.) These droplets are formed through the vigorous breakup of the oil ganglia that is caused by high-Ca flows (dynamic breakup, Payatakes 1982; Hinkley *et al.* 1982). The small oil droplets seem to be stabilized by the flow of the surrounding water and thus there is little tendency for the development of ganglia through collision/coalescence of droplets. (Sufficiently prolonged collisions that would lead to coalescence are rare.)

The domain of DTF is shown in figure 3. It corresponds to relatively high Ca and/or low S_w values, specifically, $Ca \gtrsim 5 \times 10^{-6}$ and $S_w \lesssim 55\%$. In the case of $\kappa = 3.35$, DTF appears in some cases with $Ca \approx 10^{-6}$ and $S_w \gtrsim 55\%$. As the viscosity ratio κ decreases, DTF becomes restricted to the region of higher Ca and lower S_w values. We observed that at high viscosity ratio (say, $\kappa = 3.35$), oil ganglia break more easily and form small ganglia and droplets. The oil droplets become more numerous as Ca and S_w increase. This observation explains why the domain of SGD that borders the domain of DTF becomes much narrower (virtually disappears), when κ is changed from 1.45 to 3.35.

In figures 6(*a*), (*b*) two snapshots of DTF, corresponding to the point C in figure 3,

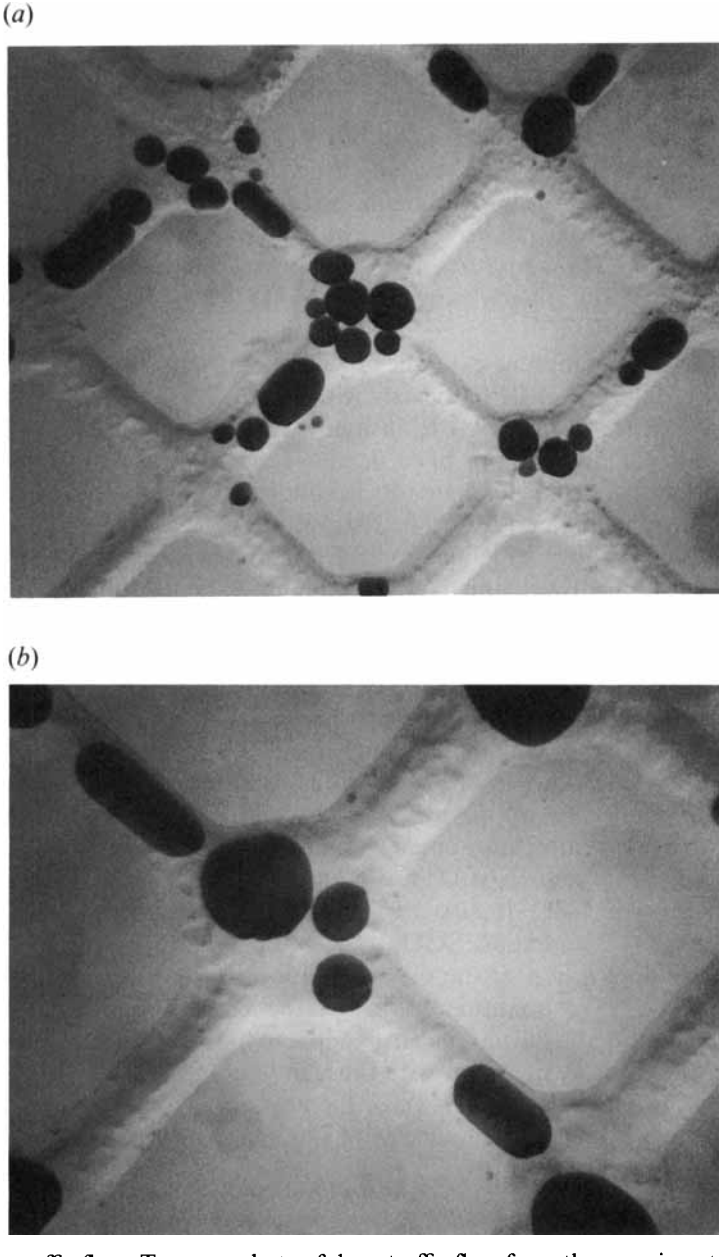

FIGURE 6. Drop-traffic flow. Two snapshots of drop traffic flow from the experiment corresponding to the point C in figure 3. (*a*) Drop-traffic flow in the region of a few pores, (*b*) oil drops inside a single chamber.

are shown. Two different levels of magnification are used to provide a clear picture of DTF on the scale of a few pores, figure 6(*a*) and inside a single chamber, figure 6(*b*).

In our experiments, a flow regime resembling flow of both phases through separate and uninterrupted pathways was observed only in the region of relative high Ca, figure 3. This regime is denoted as *connected pathway flow* (CPF). The combination of large Ca and large S_o (small S_w) values favours CPF (at least in the case of unstable fluid–fluid systems). In this flow regime, even though both phases flow mainly through

their own separate networks of interconnected pores, at the fringes of the oil pathways oil ganglia and/or droplets are being created frequently, as small amounts of oil become separated from the continuous mass of the oil. Thus, depending on the values of Ca and S_w either SGD or DTF arises in the areas between the oil pathways. This can be seen in figure 3, where the domain of CPF is adjacent to the domains of both SGD and DTF. In the case of large viscosity ratio (here $\kappa = 3.35$) CPF can only coexist with DTF because, then, any small ganglia fission readily for $Ca > 10^{-6}$.

It is worth noting that the connected pathways seem rather stable, and that they are stabilized further as the flow rates increase. Of course, the motion of the disconnected oil at the borders of the oil pathways (SGD or DTF) has its characteristic quasi-stochastic behaviour.

Figure 7 shows two different examples of CPF. In figure 7(*a*) CPF coexists with SGD, whereas in figure 7(*b*) CPF coexists with DTF. The former corresponds to the point D, and the latter to the point E, in figure 3.

A reasonable explanation of this phenomenon is as follows. At high Ca (and $\kappa > 1$) the oil ganglia have a strong tendency to follow pathways composed of large pores (Constantinides & Payatakes 1991). They also undergo vigorous fissioning (dynamic breakup). The concentration of ganglia on the large-pore pathways increases the value of S_o along those pathways. If the average value of S_o is also high, then the value of S_o along the large-pore pathways will be sufficiently high to induce frequent and relatively prolonged collisions which, when coalescence following collision is prompt (say $Co \gtrsim 0.5$), will lead to the formation of connected oil pathways. The maintenance of the connected oil pathways, when their formation is kinetically possible, is aided by the fact that it leads to much smaller mechanical energy dissipation than ganglion dynamics or drop-traffic flow. The precarious balance between the tendency for organization in connected oil pathways (through collision/coalescence), and the tendency for disorganization into small ganglia and/or droplets (through dynamic breakup) explain why a domain of DTF is interposed between the domain of ganglion dynamics and that of CPF. It also explains the fact that the spaces between oil pathways contain DTF and some SGD.

The qualitative description of the oil distribution in the various flow regimes that was given above can be quantified through the corresponding oil ganglion size distributions of stranded and mobilized ganglia. At steady-state conditions the size distribution remains nearly invariant with time. In figure 8, the size distributions of the oil ganglia (moving as well as stranded) for the flows that correspond to the points A, B and C of figure 3 are given, obtained with the image analysis process.

4.2. *Relative permeability measurements*

The conventional relative permeabilities to water and oil, k_{rw} and k_{ro}, respectively, are defined by the following phenomenological expressions:

$$q_w = \frac{kk_{rw}}{\mu_w} A \frac{\Delta P_w}{L}, \quad q_o = \frac{kk_{ro}}{\mu_o} A \frac{\Delta P_o}{L}, \tag{4a,b}$$

where, k is the absolute permeability of the model porous medium, L is the distance between the pressure taps, A is the cross-sectional area of the model porous medium (width of the network × length of periodicity = 105 mm × 1.221 mm), and ΔP_w and ΔP_o are the time-averaged hydrostatic pressure drops of water and oil, respectively. Rapid and noisy fluctuations of ΔP_w and ΔP_o were observed even at 'steady state'. These were in the range from $\pm 5\%$ to $\pm 20\%$ of the time-averaged values, depending on the flow

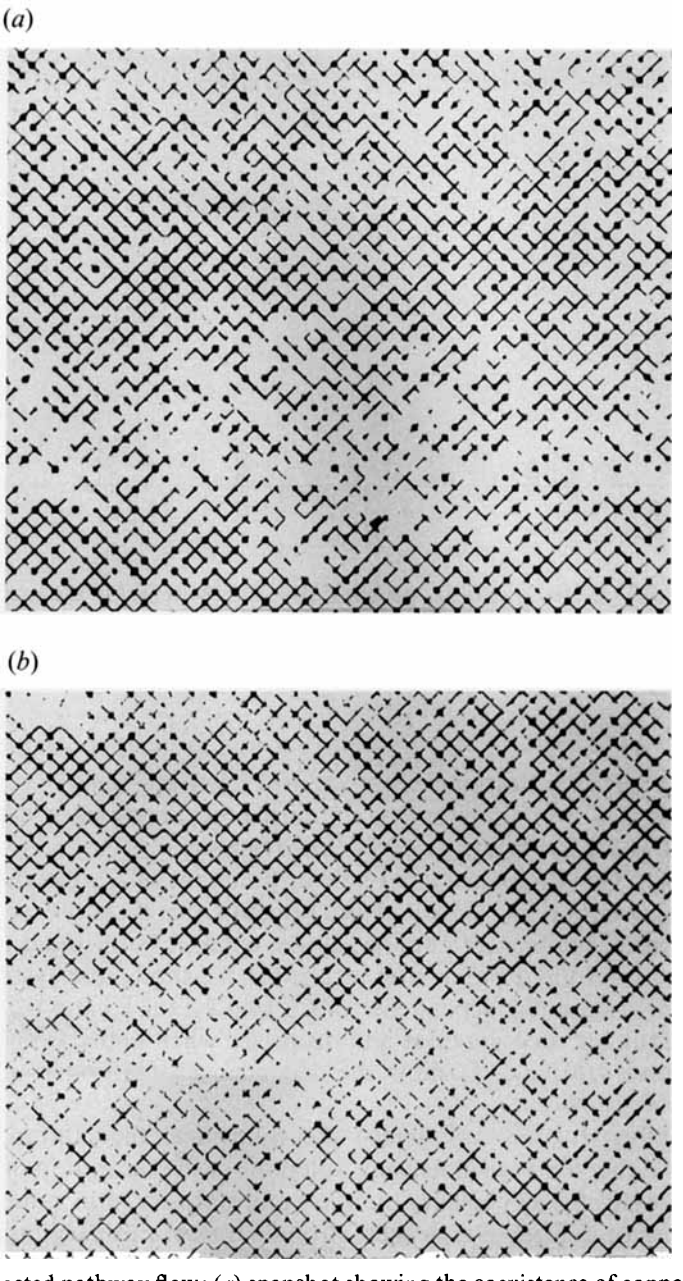

FIGURE 7. Connected pathway flow: (*a*) snapshot showing the coexistence of connected pathway flow with small ganglion dynamics, corresponding to point D in figure 3; (*b*) snapshot showing the coexistence of connected pathway flow with drop-traffic flow, corresponding to point E in figure 3.

rates of the two fluids or, alternatively, on Ca and r. Despite the fact that these fluctuations were sizeable, the time-averaged values were constant and permitted determination of the relative permeabilities with sufficient accuracy. It should be emphasized here that the observed fluctuations are not caused by an inadequacy in the size of the entire model, but that they are inherent in the two-phase flow (they are of capillary origin and are caused by the continuous motion of numerous menisci and/or

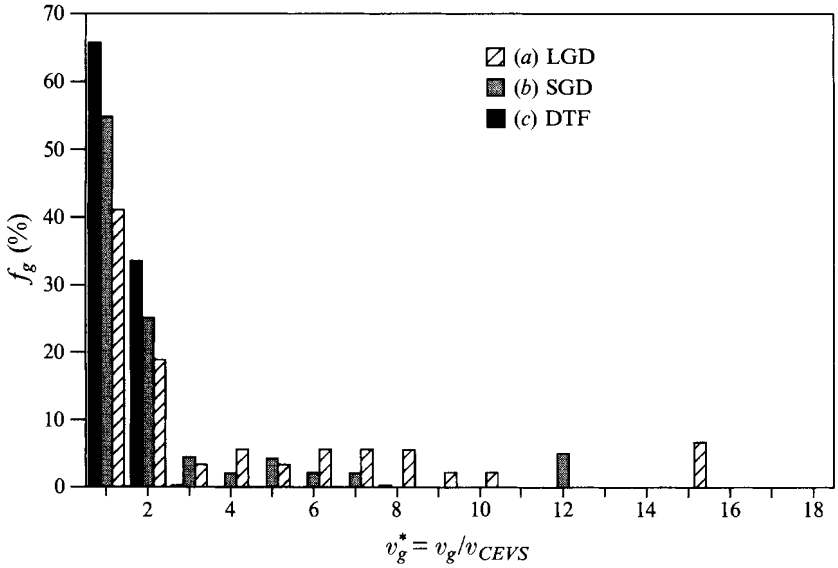

FIGURE 8. Mean (moving and stranded) ganglion size distributions for the main flow regimes, obtained with image analysis of the experiments corresponding to the points A, B and C of figure 3. Here, v_g is the ganglion volume, v_{CEVS} is the average pore-volume per node of the network, v_g^* is the reduced ganglion volume, and f_g is the percentage of ganglia with reduced volume v_g^*.

droplets through pores of varying cross-section) even at 'steady-state', when one measures the pressures over a region that contains a few hundreds of nodes or less. Of course, this scale is crucial in the study of flow regimes.

The relative permeabilities are treated here as functions of S_w, Ca and κ, according to (1) and (2). Furthermore, S_w is treated as a function of r, Ca and κ, according to (3). All the experimental results were obtained under conditions of initial imbibition.

Figure 9 presents all the experimental results for the three fluid systems used here. Figures 9(*a*), (*c*), (*e*) show the dependence of k_{rw} and k_{ro} on S_w and Ca. The viscosity ratio, κ, is constant for each diagram and decreases when going from figure 9(*a*) to figure 9(*e*). Figures 9(*b*), (*d*), (*f*) show the dependence of S_w on r and Ca, for the corresponding values of κ.

From figures 9(*a*), (*c*), (*e*), we deduce the following: the conventional relative permeabilities to either fluid are increasing functions of the saturation of the respective fluid. This result holds for all capillary numbers and viscosity ratio values investigated.

The relative permeabilities also depend strongly on the capillary number, Ca, and they increase as Ca increases. Given that in the experiments the capillary number was changed only by changing the water flow rate, q_w, keeping all other parameters constant, it follows that the relative permeabilities are increasing functions of the water flow rate. This result holds over the entire range of the saturation values measured in the present work.

The relative permeabilities tend to become linear functions of S_w as Ca increases. The relative permeability to water, k_{rw}, is a virtually linear function of S_w for all Ca values used. On the other hand, at the lowest value of the capillary number used ($Ca = 10^{-7}$) the relative permeability to oil, k_{ro}, changes more abruptly at low than at high values of S_w. At higher values of the capillary number ($Ca = 10^{-6}$ and 5×10^{-6}) k_{ro} also becomes a nearly linear function of S_w. Furthermore, for all values of Ca, the two relative

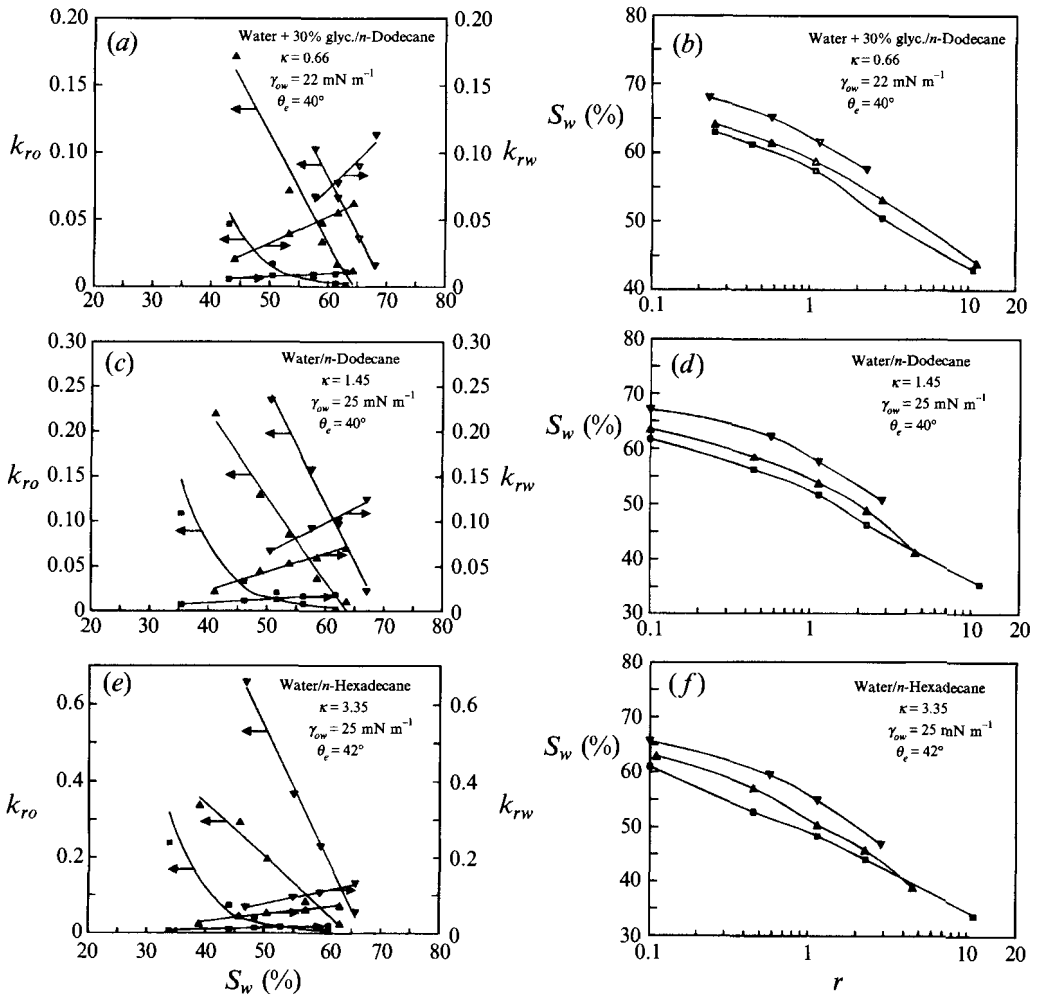

FIGURE 9. Dependence of the 'steady-state' relative permeabilities, k_{ro} and k_{rw}, and of the water saturation, S_w, on the main flow parameters. Relative permeabilities are presented as functions of S_w, Ca and κ, whereas water saturation is presented as a function of r, Ca and κ. (All the other parameters were kept constant.) □, $Ca = 10^{-7}$; △, $Ca = 10^{-6}$; ▽, $Ca = 5 \times 10^{-6}$.

permeabilities become equal (that is, the two curves cross) at a water saturation value greater than 50%, which is typical behaviour for water-wet porous media (Craig 1971).

From figures 9(*b*), (*d*), (*f*) we deduce the following:

(i) at constant Ca (that is, at constant water flow rate, q_w), S_w decreases (S_o increases) as the flow-rate ratio, $r(= q_o/q_w)$, increases (that is, as the oil flow-rate, q_o, increases);

(ii) at constant flow-rate ratio, r, S_w increases (S_o decreases) as Ca increases (that is, as the water flow rate, q_w, increases);

(iii) at constant values of Ca and r, when κ increases, S_w decreases weakly, but discernibly. A similar result has been obtained from immiscible displacement experiments: keeping constant the value of Ca, the residual oil saturation, S_{or}, increases as the viscosity ratio increases (Vizika, Avraam & Payatakes 1994). These results confirm the important role of the viscosity ratio even at very small values of the capillary number (see also Dias & Payatakes 1986*a*; Vizika & Payatakes 1989).

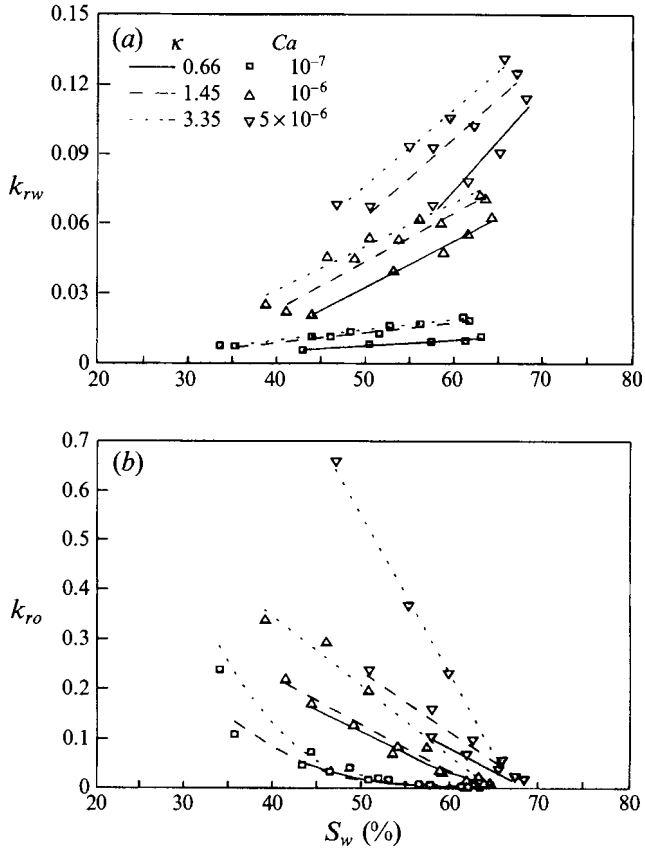

FIGURE 10. (*a*) Dependence of the 'steady-state' relative permeability to water, k_{rw}, on the viscosity ratio, κ, for three different Ca values. (*b*) Dependence of the 'steady-state' relative permeability to oil, k_{ro}, on the viscosity ratio for three different Ca values.

A summary of the relative permeabilities for all values of the capillary number and the viscosity ratio is given in figure 10. We deduce the following.

As Ca increases, both relative permeabilities become more sensitive functions of the saturation. The phenomenon is enhanced for k_{ro} as κ increases, whereas for k_{rw} as κ decreases.

The viscosity ratio, κ, also affects the relative permeabilities. As κ increases, k_{ro} increases strongly (figure 10*b*). The relative permeability to water, k_{rw}, also increases as κ increases but less strongly than k_{ro} (figure 10*a*).

4.3. *Flow regimes and relative permeabilities*

Figure 11 presents a correlation between the relative permeabilities, k_{rw} and k_{ro}, and the corresponding flow regimes. The relative permeabilities are shown as columns of the appropriate height, placed on the flow regime map.

Starting from LGD, as Ca increases with constant water saturation, S_w (which is equivalent to an increase of the water flow rate, q_w), or as S_w decreases with constant Ca (which is equivalent to an increase of the oil flow rate, q_o), or when both parameters change in these directions, the mean ganglion size decreases. Consequently, the flow regime changes from LGD, through SGD, to DTF. At even higher values of Ca the oil is forced to develop connected pathways, while SGD and/or DTF still

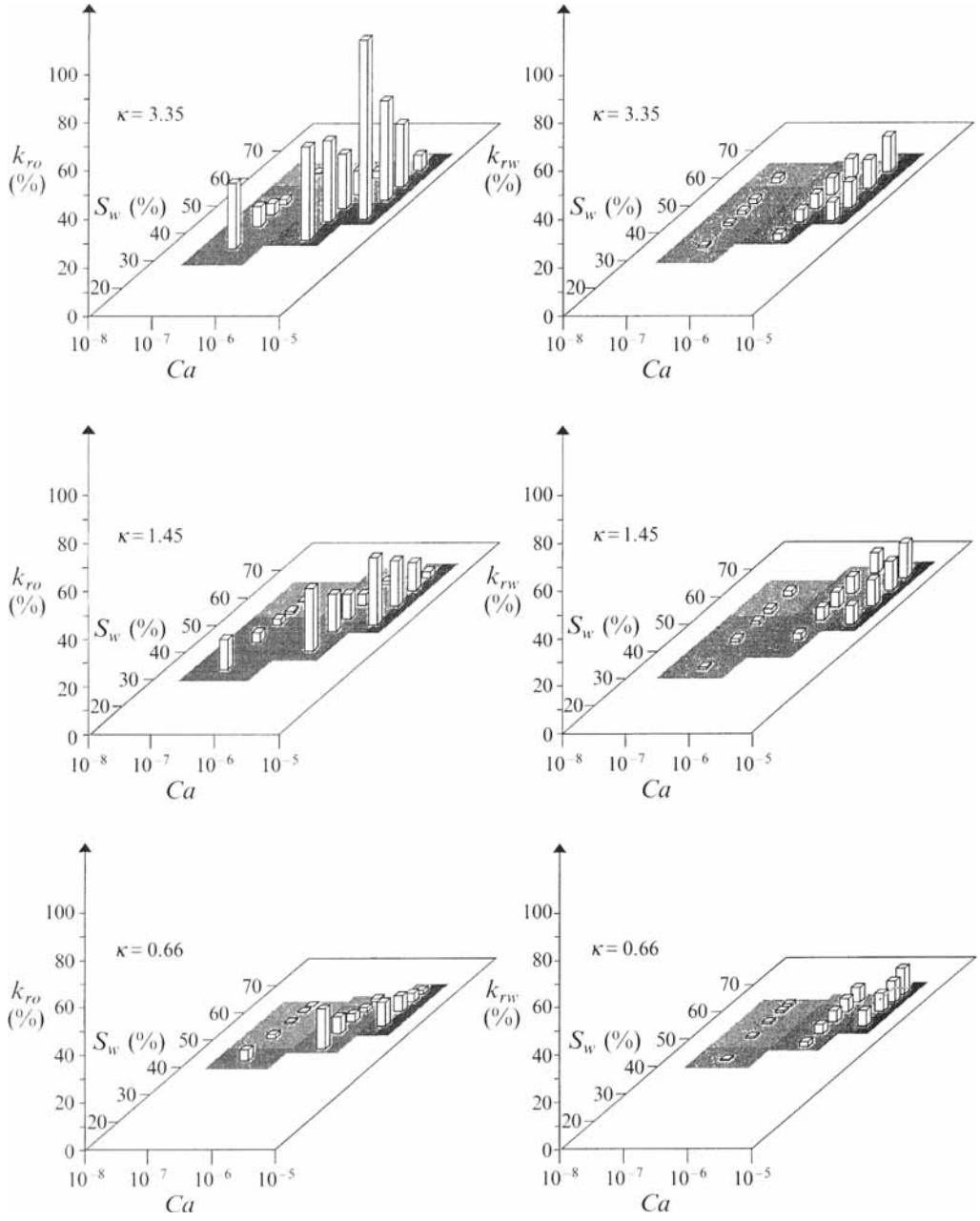

FIGURE 11. Map of flow regimes and 'steady-state' relative permeabilities. The 'steady-state' relative permeabilities, k_{ro} and k_{rw}, show a strong correlation with the flow regimes. (See the text for a discussion of mechanisms.)

persist mainly at the fringes of the oil pathways. Consequently, as Ca increases and/or S_w decreases, the relative permeability to oil, k_{ro}, increases. The relative permeability to water, k_{rw}, increases with increasing Ca, but it decreases as S_w decreases (while keeping Ca constant).

When the flow regime is LGD, most of the pores of the network remain blocked (for large lengths of time, or even permanently) by stranded small ganglia. Oil flows in the

form of large ganglia, and only a few small ganglia are mobilized, usually when large ganglia pass near them or collide with them. Under these conditions, a large pressure drop is needed to mobilize even a small amount of oil, and the oil flow rate is small. Consequently, the relative permeabilities to both fluids are low in the domain of LGD.

When the flow regime is SGD, a substantial fraction of the population of small ganglia are mobilized (moving with velocities that are slightly lower than those of large ganglia). Under such conditions, most of the pores of the network do not remain blocked for a long time. The paths that are followed by the moving oil ganglia carry not only oil but also water (in between oil ganglia and, possibly, along the wetting films). Because, of this, considerable amounts of disconnected oil and of connected (as well as of nearly disconnected) water flow under the influence of the applied macroscopic pressure gradient. Consequently, the relative permeabilities to both phases are substantially higher than those obtained with LGD.

When the flow regime is DTF, the small oil drops move with very high velocities (comparable to the mean interstitial velocity of the water), while they have small probability to be stranded. The combination of high flow rates for both fluids, and of relatively small flow resistances lead to high values of the relative permeabilities to both fluids. When the conditions induce CPF (combined with some SGD or DTF), the flow of each fluid approaches the mode of one-phase flow. In this regime the relative permeability to oil takes the largest values measured in all the experiments. The relative permeability to water is also large and increases as the water saturation increases.

The viscosity ratio, κ, also affects the flow mechanisms and the relative permeabilities. As κ increases with constant Ca, the oil saturation, S_o, attained at steady-state increases (figures 9*b*, *d*, *f*). The increase of κ also favours the formation of small oil ganglia and oil drops. This leads to an expansion of the domains of SGD and DTF, figure 3. For the same reason, the relative permeabilities for large κ are higher than those for low κ, figure 11.

When the viscosity ratio is quite large (say, $\kappa = 3.35$) a lubricating thin layer of the wetting fluid covering the pore walls is developed (Yuster 1951; Odeh 1959). Formation of wetting films is facilitated by the microroughness of the pore walls. When this happens the oil behaves as if it had an effective viscosity smaller than its bulk value (Dullien 1979). It is generally assumed that the wetting films have such a small thickness that they do not contribute to the flow rate of the water. However, we measured a small but discernible increase of the relative permeability to water for $\kappa = 3.35$, which may be caused by the flow of wetting films.

4.4. *Fractional flow measurements*

When steady-state conditions are established, the fractional flow can be determined from its definition

$$f_w = \frac{q_w}{q_w + q_o} = \frac{1}{1+r}. \tag{5}$$

At steady-state conditions the time-averaged fluid flow rates, q_w and q_o, are constant at every cross-section of the porous medium, and f_w corresponds to a single value of the fluid saturation S_w.

Figure 12 gives f_w as a function of the water saturation, S_w, for all values of the capillary number, Ca, and the viscosity ratio, κ, used in the experiments. These curves of f_w *vs.* S_w are quite similar to those used in industrial practice. However, it turns out that f_w depends strongly not only on S_w but also on Ca and κ (with all other geometrical and physical parameters kept constant).

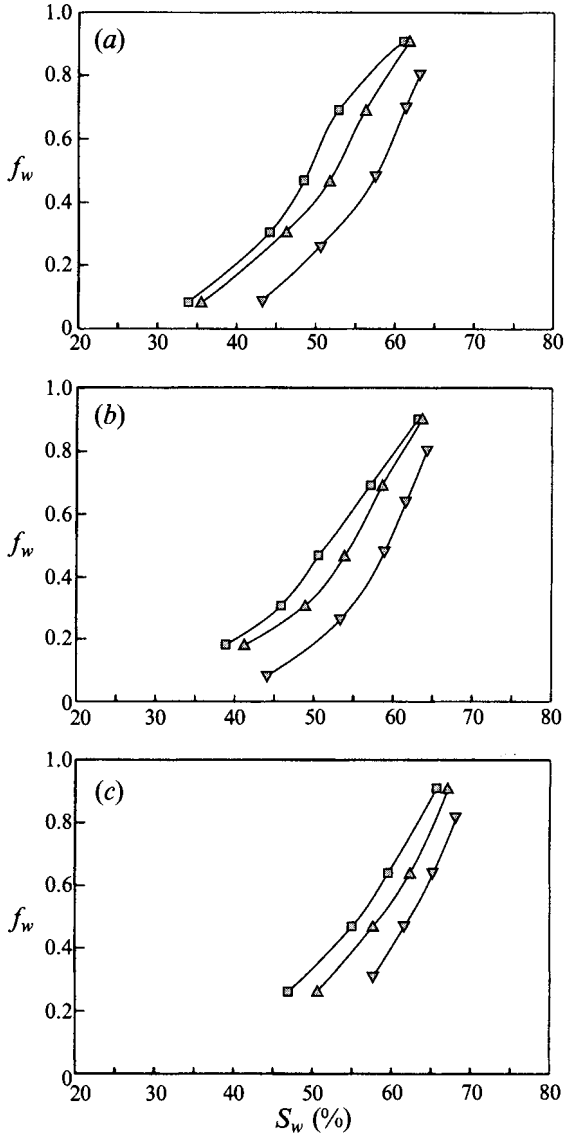

FIGURE 12. Dependence of the fractional flow, f_w, on the capillary number, Ca, and the viscosity ratio, κ. (*a*) $Ca = 10^{-7}$, (*b*) $Ca = 10^{-6}$, (*c*) $Ca = 5 \times 10^{-6}$; κ = □, 3.35; △, 1.45; ▽, 0.66.

Figure 12 shows that f_w decreases as Ca increases, when κ and S_w are kept constant. On the other hand, f_w increases as κ increases, when Ca and S_w are kept constant.

As Ca increases and/or κ decreases, the curves $\{f_w \; vs. \; S_w\}$ tend to abandon the typical s-shape and to become concave upward. In the case of concave upward $\{f_w \; vs. \; S_w\}$ curves, the conventional Buckley–Leverett theory for linear displacement predicts the development of a water saturation discontinuity at the flow front. However, we do not expect that the conventional fractional flow theory holds at the flood front, where the capillary effects are dominant and the saturation gradients are both steep and fuzzy (see also Payatakes & Dias 1984).

5. Conclusions

Steady-state two-phase flow was studied experimentally in a planar model pore network of the chamber-and-throat type, etched in glass. The capillary number, Ca, the flow-rate ratio, r, and the viscosity ratio, κ, were changed systematically, whereas the wettability (equilibrium contact angle $\theta_e \approx 40°$) and the geometrical and topological parameters of the porous medium were kept constant. In all the experiments coalescence, given a collision between ganglia, was prompt (large coalescence factor, Co). The flow history in all the experiments was initial imbibition.

The flow mechanisms at the pore-scale and the macroscopic flow regimes were observed under 'steady-state' conditions. The flow regimes were correlated with the corresponding values of the pertinent flow parameters, Ca, S_w and κ. The macroscopic conventional relative permeabilities of the two fluids, k_{rw}, and k_{ro}, were measured as functions of the flow parameters and correlated with the flow regimes. The main conclusions are the following.

(i) During steady-state two-phase flow, and over broad ranges of the pertinent dimensionless parameters (say, $10^{-8} \lesssim Ca \lesssim 10^{-6}$, $0.6 \lesssim \kappa \lesssim 3.4$, $20\% \lesssim S_w \lesssim 80\%$, and with all the other physical, geometrical and topological parameters fixed) the oil (non-wetting fluid) is disconnected in the form of ganglia and/or droplets. The water (wetting fluid) preserves its connectivity by forming an ever-changing network of connected pathways, as well as of wetting films. Wetting films become interposed between the oil and the pore walls, taking advantage of the wall microroughness. (We expect that these observations hold even in some areas that are outside the parameter ranges which were investigated, say $Ca < 10^{-8}$, $\kappa \lesssim 0.6$, and $\kappa > 3.4$.) Flow of the oil, despite its disconnected form, takes place through the motion of some (or all) of the ganglia, in a process that is denoted as *steady-state ganglion dynamics*. On the scale of a few pores this process is inherently transient. On the mesoscale the process is 'noisy' but stationary, and can be characterized as steady state.

(ii) Motion of ganglia in low-Ca flows is possible because the critical condition for the mobilization of any given ganglion is that the corresponding *ganglion mobilization number* be larger than unity, $Gm > 1$. This is possible even in low-Ca flows, especially when k_{rw} is sufficiently small.

(iii) Connected oil pathways were observed only for relatively high Ca values, say when $Ca \gtrsim 5 \times 10^{-6}$. Formation of connected oil pathways is favoured by a combination of high $\kappa (= \mu_o/\mu_w)$ and large S_o (small S_w) values.

(iv) The foregoing experimental results necessitate a drastic and highly important revision of the long-held dogma, which presumed that in steady-state two-phase flow both fluids move only through connected pathways, and that any disconnected bodies of oil remain stranded. This new insight is expected to have profound implications for the consistent mathematical treatment of the process.

(v) The distribution of the oil can be characterized by the *time-averaged mean size* of the *mobilized* ganglia (or droplets). Based on this criterion, four main flow regimes have been identified, namely, large-ganglion dynamics (LGD), small-ganglion dynamics (SGD), drop-traffic flow (DTF), and connected pathway flow (CPF). The flow regime that is obtained during steady-state flow depends on the values of Ca, S_w (or r), and κ (keeping the wettability and all the other physical, geometrical and topological parameters constant).

(vi) A map of the flow regimes is given in figure 3. The domain of LGD corresponds to small Ca and medium-to-large S_w values. This domain increases appreciably when κ decreases. The domain of SGD is adjacent to that of LGD, on the side of larger

values of Ca and/or smaller values of S_w. This domain also increases when κ decreases (from 3.35 to 1.45), but decreases again as κ decreases further (from 1.45 to 0.66). The domain of DTF is adjacent to that of SGD, on the side of larger Ca and/or smaller S_w values. This domain decreases as κ decreases. The domain of CPF corresponds to medium and high Ca values (say, $Ca \gtrsim 5 \times 10^{-6}$) and, for large κ values, it is enhanced by large S_o (small S_w) values. A qualitative mechanistic explanation for this flow behaviour is given in the main part of this work.

(vii) The boundaries between the flow regimes are fuzzy. Each regime merges with its neighbour(s) gradually. In particular, in all our experiments CPF was accompanied by elements of DTF and/or SGD. (Mobilized droplets and/or small ganglia are formed along the fringes of the connected oil pathways, and contribute to the overall oil flow rate.)

(viii) The relative permeability to oil, k_{ro}, correlates strongly with the flow regimes, figure 11. It is minimal in the domain of LGD, and increases strongly as the flow mechanism changes from LGD to SGD to DTF to CPF. A qualitative mechanistic explanation of this behaviour is given in the main part of this work. (A network-type computer simulator of LGD and SGD that describes this behaviour quantitatively is developed in Constantinides & Payatakes 1995.)

(ix) The relative permeability to water, k_{rw}, also correlates with the flow regimes, figure 11. It is minimal in the domain of SGD. It increases moderately as the flow mechanism changes from SGD to LGD. It increases strongly as the flow mechanism changes from SGD to DTF and CPF.

(x) Both relative permeabilities are functions not only of S_w, but also of Ca and κ (with all other parameters fixed).

(xi) For constant κ, k_{ro} increases strongly as Ca increases and/or as S_w decreases (S_o increases). For constant Ca and S_w, k_{ro} increases strongly as κ increases.

(xii) For constant κ, k_{rw}, increases strongly as Ca increases and/or as S_w increases. For constant κ, k_{rw} increases moderately as κ increases.

(xiii) Both k_{ro} and k_{rw} increase strongly as the water flow rate, q_w, increases while q_o is kept constant (that is, as r decreases). We consider this as strong evidence of the existence of coupling effects.

(xiv) The fact that both k_{ro} and k_{rw} increase as κ increases (for $\kappa > 1$) is a possible indication that the wetting films thicken as κ increases, and that this creates a strong lubrication effect for the non-wetting fluid.

(xv) The water saturation, S_w, is an increasing function of Ca, a decreasing function of r, and a decreasing function of κ.

(xvi) The fractional flow of water, f_w, is not only a function of the water saturation, S_w, but also a strong function of Ca and κ (with the wettability and all other parameters kept constant), figure 12.

(xvii) The strong dependence of f_w, k_{ro}, and k_{rw} not only on S_w, but also on Ca and κ (with the wettability, the coalescence factor, and all the other parameters kept constant) implies that a fundamental revamping of conventional fractional flow theory is warranted. Indeed, it is neither consistent nor satisfactory to rely on a model in which the parameters that are used to predict the flow rates of the two fluids depend very strongly on the flow rates themselves, as well as on a number of other flow-related quantities (κ, Co, etc.).

This work was supported by Shell Research BV, Koninklijke/Shell-Exploratie en Produktie Laboratorium (KSEPL), and by the Institute of Chemical Engineering and High Temperature Chemical Processes. We thank the ex-undergraduates A. Vlassis,

P. Karfakis, I. Papantoniou, T. Skoumba, S. Pelekasi, V. Anagnostopoulou and S. Malakasi for their valuable help in the experiments. We also thank Professor Ioannis Chatzis, University of Waterloo, for useful discussions. Parts of this work and videotaped experiments were presented at the Gordon Research Conference on 'Modeling of Flow in Permeable Media', Plymouth State College, N.H., Aug. 10–14, 1992.

REFERENCES

ADLER, P. M. & BRENNER, H. 1988 Multiphase flow in porous media. *Ann. Rev. Fluid. Med.* **20**, 35.

AMAEFULE, J. O. & HANDY, L. L. 1982 The effects of interfacial tensions on relative oil/water permeabilities of consolidated porous media. *Soc. Petrol. Engrs J.* **22**, 371.

AURIAULT, J.-L. 1987 Nonsaturated deformable porous media: quasastatics. *Transport in Porous Media* **2**, 45.

AURIAULT, J.-L., LEBAIGUE, O. & BONNET, G. 1989 Dynamics of two immiscible fluids flowing through deformable porous media. *Transport in Porous Media* **4**, 105.

AVRAAM, D. G., KOLONIS, G. B., ROUMELIOTIS, T. C., CONSTANTINIDES, G. N. & PAYATAKES, A. C. 1994 Steady-state two-phase flow through planar and non-planar model porous media. *Transport in Porous Media* **16**, 75.

BENTSEN, R. G. 1974 Conditions under which the capillary term may be neglected. *J. Can. Petrol. Tech.* Oct.–Dec., 25.

BUCKLEY, S. E. & LEVERETT, M. C. 1942 Mechanism of fluid displacement in sands. *Trans. AIME* **146**, 107.

CHATZIS, J. D., MORROW, N. R. & LIM, H. T. 1983 Magnitude and detailed structure of residual oil saturation. *Soc. Petrol. Engrs J.* **23**, 311.

CONSTANTINIDES, G. N. & PAYATAKES, A. C. 1991 A theoretical model of collision and coalescence of ganglia in porous media. *J. Colloid Interface. Sci.* **141**(2), 486.

CONSTANTINIDES, G. N. & PAYATAKES, A. C. 1995 Network simulation of steady-state two-phase flow in consolidated porous media. *AIChE J.* (in press).

CRAIG, F. F. 1971 The reservoir engineering aspects of waterflooding. *Soc. Petrol. Engrs AIME* Monograph Vol. 3.

CRUZ, V. DE LA. & SPANOS, T. J. T. 1983 Mobilization of oil ganglia. *AIChE J.* **29**, 854.

DIAS, M. M. & PAYATAKES, A. C. 1986*a* Network models for two-phase flow in porous media. Part 1. Immiscible microdisplacement of non-wetting fluids. *J. Fluid Mech.* **164**, 305.

DIAS, M. M. & PAYATAKES, A. C. 1986*b* Network models for two-phase flow in porous media. Part 2. Motion of oil ganglia. *J. Fluid Mech.* **164**, 337.

DULLIEN, F. A. L. 1978 *Porous Media. Fluid Transport and Pore Structure.* Academic.

FULCHER, G. A., ERTEKIN, T. & STAHL, C. D. 1985 Effect of capillary number and its constituents on non-phase relative permeability measurements. *J. Petrol. Tech.* Feb., 249.

GEFFEN, T. M., OWENS, W. W., PARRISH, D. R. & MORSE, R. A. 1951 Experimental investigation of factors affecting laboratory relative permeability measurements. *Petrol. Trans. AIME* **192**, 99.

GENNES, P. G. DE. 1983 Theory of slow biphasic flows in porous media. *Phys. Chem. Hydrodyn.* **4**, 175.

HEAVYSIDE, J., BLACK, C. J. J. & BERRY, J. F. 1983 Fundamentals of relative permeability: Experimental and theoretical considerations. *58th Annual Technical Conference and Exhibition, San Francisco, CA. October 5–8, Paper SPE* 12173.

HINKLEY, R. E., DIAS, M. M. & PAYATAKES, A. C. 1987 On the motion of oil ganglia in porous media. *Phys. Chem. Hydrodyn.* **8** (2), 185.

HONARPOOR, M. & MAHMOOD, S. M. 1988 Relative-permeability measurements: An overview. *J. Petrol. Tech.* Aug., 963.

JERAULT, G. R. & SALTER, S. J. 1990 The effect of pore structure on hysteresis in relative permeability and capillary pressure: Pore-level modeling. *Transport in Porous Media* **5**, 103.

JOHNSON, E. F., BOSSLER, D. R. & NAUMANN, V. O. 1959 Calculation of relative permeability from displacement experiments *J. Petrol. Tech.* Jan., 61.

JONES, S. C. & ROSZELLE, W. O. 1978 Graphical techniques for determining relative permeability from displacement experiments. *J. Petrol. Tech.* May, 807.

JONES-PARA, J. & CALHOUN, J. C. 1953 Computation of a linear flood by the stabilized core method. *Trans. AIME* **198**, 335.

KALAYDJIAN, F. 1987 A macroscopic description of multiphase flow in porous media involving evolution of fluid/fluid interface. *Transport in Porous Media* **2**, 537.

KALAYDJIAN, F. 1990 Origin and quantification of coupling between relative permeabilities for two-phase flows in porous media. *Transport in Porous Media* **5**, 215.

LEFEBVRE DU PREY, E. J. 1973 Factors affecting liquid–liquid relative permeabilities of a consolidated porous medium. *Soc. Petrol. Engrs. J.* Feb., 39.

LEVERETT, M. C. 1941 Capillary behavior in porous solids. *Trans. AIME* **142**, 152.

LEVINE, J. S. 1954 Displacement experiments in a consolidated porous system. *Trans. AIME* **201**, 57.

MCCAFFERY, F. G. & BENNION, D. W. 1974 The effect of wettability on two-phase relative permeabilities. *J. Can. Petrol. Tech.* Oct.–Dec., 42.

MORSE, R. A., TERWILLIGER, P. L. & YUSTER, S. T. 1947 Relative permeability measurements on small core samples. *Oil Gas J.* Aug., 23.

NAAR, J., WYGAL, G. R. & HENDERSON, J. H. 1962 Imbibition relative permeability in unconsolidated porous media. *Soc. Petrol. Engrs. J.* **2**, 13.

NG, K. M., DAVIS, H. T. & SCRIVEN, L. E. 1978 Visualization of blob mechanisms in flow through porous media. *Chem. Engng Sci.* **33**, 1009.

NG, K. M. & PAYATAKES, A. C. 1980 Stochastic simulation of the motion, breakup and stranding of oil ganglia in water-wet granular porous media during immiscible displacement. *AIChE J.* **26**, 419.

ODEH, A. S. 1958 Effect of viscosity ratio on relative permeability. *J. Petrol. Tech.* **11**, 346.

OSOBA, J. S., RICHARDSON, J. G., KERVER, J. K., HAFFORD, J. A. & BLAIR, P. M. 1951 Laboratory measurements of relative permeability. *Trans. AIME* **192**, 47.

OWENS, W. W. & ARCHER, D. L. 1971 The effect of rock wettability on oil-water relative permeability relationships. *J. Petrol. Tech.* July, 873.

PAYATAKES, A. C. 1982 Dynamics of oil ganglia during immiscible displacement in water-wet porous media. *Ann. Rev. Fluid Mech.* **14**, 365.

PAYATAKES, A. C. & DIAS, M. M. 1984 Immiscible microdisplacement and ganglion dynamics in porous media. *Rev. Chem. Engng* **2**, 85.

PAYATAKES, A. C., NG, K. M. & FLUMERFELT, R. W. 1980 Oil ganglion dynamics during immiscible displacement: Model formulation. *AIChE J.* **26**, 430.

PHILIP, J. R. 1970 Flow in porous media. *Ann. Rev. Fluid Mech.* **2**, 177.

RAATS, P. A. & KLUTE, A. 1968 Transport in soils: the balance of momentum. *Soil Sci. Soc. Am. J.* **32**, 452.

RAPIN, S. 1980 Behavior of non-wetting oil ganglia displaced by an aqueous phase. MSc thesis, University of Houston.

RAPOPORT, L. A. & LEAS, W. J. 1953 Properties of linear waterfloods. *Trans. AIME* **198**, 139.

RICHARDS, L. A. 1931 Capillary conduction of liquids through porous mediums. *Physics* **1**, 318.

RICHARDSON, J. G., KERVER, J. K., HAFFORD, J. A. & OSOBA, J. S. 1952 Laboratory determination of relative permeability. *Trans. AIME* **195**, 187.

ROSE, W. 1972 *Fundamentals of Transport Phenomena in Porous Media.* IAHR, Elsevier.

ROSE, W. 1988 Measuring transport coefficients necessary for the description of coupled two-phase flow of immiscible fluids in porous media. *Transport in Porous Media* **3**, 163.

ROSE, W. 1990 Coupling coefficients for two-phase flow in pore spaces of simple geometry. *Transport in Porous Media* **5**, 97.

ROSE, W. 1991 Richard's assumptions and Hassler's presumptions. *Transport in Porous Media* **6**, 91.

SANDBERG, C. R., GOURNAY, L. S. & SIPPEL, R. F. 1958 The effect of fluid-flow rate and viscosity on laboratory determinations of oil-water relative permeabilities. *Petrol. Trans. AIME* **213**, 36.

TABER, J. J. 1958 The injection of detergent slugs in water floods. *Trans. AIME* **213**, 186.

TERWILLIGER, P. L., WILSEY, L. E., HALL, H. N., BRIDGES, P. M. & MORSE, R. A. 1951 An

experimental and theoretical investigation of gravity drainage performance. *Trans. AIME* **192**, 285.

VIZIKA, O., AVRAAM, D. G. & PAYATAKES, A. C. 1994 On the role of viscosity ratio during low capillary number forced imbibition in porous media. *J. Colloid Interface Sci.* **165**, 386.

VIZIKA, O. & PAYATAKES, A. C. 1989 Parametric experimental study of forced imbibition in porous media. *Phys. Chem. Hydrodyn.* **11**, 187.

WELGE, H. J. 1952 A simplified method for computing oil recovery by gas or water drive. *Trans. AIME* **195**, 91.

WHITAKER, S. 1986 Flow in porous media II: The governing equations for immiscible two-phase flow. *Transport in Porous Media* **1**, 105.

WOODING, R. A. & MOREL-SEYTOUX, H. J. 1976 Multiphase flow through porous media. *Ann. Rev. Fluid Mech.* **8**, 233.

YUSTER, S. T. 1951 Theoretical consideration of multiphase flow in idealized capillary systems. *World Petroleum Cong. Proc., Section II. Drilling and Production. The Hague.*